

Seasonality and spatial distribution of solar radiation under Arctic sea ice

Master thesis

submitted by

Stefanie Arndt

supervisors: Prof. Dr. Martin Claußen
[**Universität Hamburg**, Department of Geosciences]

Dr. Marcel Nicolaus
[**Alfred-Wegener-Institut Helmholtz-Zentrum
für Polar- und Meeresforschung**, Bremerhaven,
Department of Climate Science, Section: Sea Ice
Physics]

Meteorologisches Institut
Fachbereich Geowissenschaften
Universität Hamburg

Hamburg, May 2013

Abstract

Arctic sea ice extent decreased considerably along with the ice cover becoming thinner and more seasonal during the last decades. These observed changes have a strong impact on interactions between atmosphere and ocean and thus play a major role in Earth's climate system.

Until now, it is not possible to quantify shortwave energy fluxes through sea ice sufficiently well over large regions and during different seasons. In order to obtain Arctic-wide estimates of solar radiation under sea ice, new methods are necessary. In this thesis, an upscaling method combining a newly developed parameterization of light transmittance and remote sensing and reanalysis data is presented.

The main result suggests that 96 % of the total annual solar heat input under Arctic sea ice occurs in the time from May to August, hence in the course of only four months of the year. Sensitivity studies indicate that once the melt season begins two weeks earlier, an increase by 20 % of the total annual solar heat input through sea ice is shown. Therefore, the transition period from spring to summer, particularly the timing of the melt season, substantially affects the light availability under ice. Furthermore, a more seasonal ice cover and a higher melt pond coverage lead to higher fraction of solar radiation being transmitted through the sea ice in summer. This positive correlation between enhanced melting and increasing transmittance can be described as 'transmittance-melt feedback'.

Assuming an ongoing ice thinning, the transmittance-melt feedback results in a further increase in transmitted and absorbed heat fluxes. Changes in timing and amount of light penetrating through Arctic sea ice might also influence melt season, biological and geochemical processes as well as basal and internal melt and freeze rates. These positive feedbacks affect the mass and energy budget of sea ice and alter crucially the interaction of atmosphere and the upper ocean.

Contents

List of Symbols	i
1. Introduction and motivation	1
1.1. Sea ice: A component of the climate system	1
1.2. Changes in sea ice extent and sea ice age during the last decades . . .	3
1.3. Background and motivation for this thesis	4
2. Theoretical background	7
2.1. Optical sea ice properties	7
2.1.1. Inherent optical properties	7
2.1.2. Apparent optical properties	8
2.2. Calculation of radiative fluxes under Arctic sea ice	9
2.3. Thermodynamics of sea ice - Surface energy budget	12
3. Data and methods	15
3.1. Data description	15
3.2. Calculation of light transmission through Arctic sea ice during Au- gust 2011	18
3.3. Newly developed method for seasonality of transmittance	21
3.3.1. Improved spatial distribution of melt ponds	22
3.3.2. Ice type classification	23
3.3.3. Melt and freeze phases	24
3.3.4. Sea ice surface properties	25
3.3.5. Development of seasonal transmittance of Arctic sea ice	28
4. Results	37
4.1. Light distribution under Arctic sea ice during August 2011	37
4.2. Seasonality of solar radiation under Arctic sea ice	40
4.3. Development of light transmission from 1979 to 2011	43

4.4. Validation and sensitivity studies	46
4.4.1. Product validation using additional field data (Tara drift, 2007)	46
4.4.2. Sensitivity study I: Changing length of melt season	49
4.4.3. Sensitivity study II: Changing transmittance and melt pond fraction	51
5. Discussion and conclusions	57
5.1. Seasonality of light transmission	57
5.2. Weaknesses and possible improvements of the presented method . . .	59
5.3. Trends of light transmission from 1979 to 2011 and future implications	61
A. Regions of the Arctic Ocean	I
B. Seasonality of sea ice concentration and surface solar radiation in 2011	II
C. Mean total surface solar irradiance from 1979 to 2011	V
List of Figures	VII
List of Tables	IX
Bibliography	XI

List of Symbols

AMSR-E		Advanced Microwave Scanning Radiometer - Earth Observation System
$\alpha(\lambda, t)$		spectral albedo
$\alpha(t)$		wavelength-integrated albedo
C_i	$\text{m}^2 \text{m}^{-2}$	sea ice concentration
C_{mp}	$\text{m}^2 \text{m}^{-2}$	melt pond fraction
E_d	Wm^{-2}	downwelling irradiance
E_i	Wm^{-2}	transmitted downwelling irradiance through bare/white ice
E_{mp}	Wm^{-2}	transmitted downwelling irradiance through melt ponds
E_o	Wm^{-2}	transmitted downwelling irradiance through open water
E_T	Wm^{-2}	transmitted downwelling irradiance
E_u	Wm^{-2}	upwelling irradiance
ECMWF		European Centre for Medium-Range Weather Forecast
EFO		early freeze onset
EMO		early melt onset
FO		freeze onset
FYI		first year ice
ICDC		Integrated Climate Data Center
MO		melt onset
MODIS		Moderate Resolution Image Spectrometer
MYI		multi year ice
NSIDC		National Snow and Ice Data Center
OSI SAF		Ocean and Sea Ice Satellite Application Facilities
SSM/I		Special Sensor Microwave/Imager
$\tau(\lambda, t)$		spectral transmittance
$\tau(t)$		wavelength-integrated transmittance
τ_a		Arctic-wide mean transmittance
τ_i		transmittance of sea ice
$\tau_{i,s}$		transmittance of the mixed system of sea ice and melt ponds
τ_{mp}		transmittance of melt ponds
τ_o		transmittance of open water
ROV		remotely operated vehicle

1 | Introduction and motivation

1.1. Sea ice: A component of the climate system

Earth's climate system is modeled by decomposition into its major constituents atmosphere, ocean, biosphere, pedosphere and cryosphere and their coupling. Interactions between atmosphere and the ocean, which covers about 70 % of the Earth's surface [Lutgens et al., 1995], are crucial to the whole system. Their mutual exchange of energy and matter determines environmental conditions. The interactions involving the ocean depend substantially on its surface conditions, including a possible sea ice cover at higher latitudes of both hemispheres. Sea ice covers approximately 7.3 % of the Earth's surface and 11.8 % of the total ocean surface [Weeks, 2010]. As sea ice cover alters the interaction between atmosphere and the underlying ocean, understanding its effects through various spatial scales is necessary [Kwok & Untersteiner, 2011].

During the phase transition from liquid sea water to the solid state of sea ice, the salt dissolved in the sea is not incorporated into the newly formed ice, but rather stored in brine pockets which make the sea water saltier. Sea ice salinity is just about 3 to 12. Hence, sea ice formation increases salinity and density of the upper ocean layer, it leads to an unstable vertical density stratification, which in turn drives convective mixing (*thermohaline circulation*). Conversely, sea ice melting leads to significant fresh water input to the upper ocean layer, stabilizing the stratification and reducing convection. [Perovich & Richter-Menge, 2009]. Thus, sea ice plays a central role in vertical current pattern formation. Sea ice motion driven by wind and ocean currents thereby acts as engine of freshwater redistribution in the Arctic ocean. In addition, this fresh water input implies a strong negative latent heat flux for the region. Hence, sea ice is not only driving and changing oceanic currents but alters also atmospheric fluxes in interconnections [Perovich & Richter-Menge, 2009; Harder et al., 1998].

Sea ice insulates relatively warm ocean water from the cold lower atmosphere and

thus, decreases latent and sensible heat exchange. A thin layer of ice already effectively disrupts the heat flux (down to 10 W m^{-2}), whereas it can rise to up to 1000 W m^{-2} during summer time in regions without complete ice cover [Maykut, 1978, 1986].

In addition, the mostly snow-covered sea ice is characterized by high backscattering of sunlight (*albedo*). Incoming shortwave radiation is mostly absorbed by the ice-free ocean but in large parts reflected by sea ice. Studies examining the annual cycle of Arctic sea ice albedo have been carried out by Perovich et al. [2002] and Perovich & Polashenski [2012], taking into account thinner seasonal ice and thicker multi year ice separately. For both categories, the spring to fall albedo is predominantly governed by snow cover and melt pond fraction on top of the sea ice. Reflectivity of sea ice, or its deduced transmittance, and total incoming radiation determine the under ice radiative fluxes. Transmitted solar heat input eventually accounts for warming of the upper ocean and melting at the bottom of the ice cover, and controls oceanic biological activity as the primary forcing. Systematic measurements of radiative fluxes and the derived optical properties of sea ice, though limited in temporal and spatial coverage, have been reported from field campaigns, including the Surface Heat Budget of the Arctic Ocean (SHEBA) field experiments (1997-1998) [Perovich, 2005], the Transpolar Drift (Tara) in 2007 [Nicolaus et al., 2010a] and the transpolar cruise TransArc in 2011 [Nicolaus et al., 2012]. The transmitted solar heat input is finally available for warming of the upper ocean as well as for melting at the bottom of the ice cover and has a major bearing on oceanic biological activity as the primary productivity [Nicolaus et al., 2010a].

The variety of processes related to sea ice alludes to its importance in Earth's climate system. Additionally, sea ice serves as an indicator for ongoing climate change, for its sensitive reaction even to small changes regarding ocean or atmosphere. Locally restricted changes in sea ice configuration translate to an altered global climate through the worldwide atmospheric and oceanic circulations. The respective phenomena related to changes in global climate are subsumed as *Arctic amplification*, referring to the warming of the Arctic proceeding twice as rapidly as the average warming over the whole Northern hemisphere in the course of the past decade [Francis & Vavrus, 2012]. Some of the feedback processes involved therein, as well as implications of altered exchange behaviour at the ocean-atmosphere boundary, are presented in the following. Modifications of circulation dynamics are briefly discussed.

1.2. Changes in sea ice extent and sea ice age during the last decades

As outlined above, sea ice is quite sensitive to changes in the atmosphere and the ocean. Considering the trend of sea ice extent over the past 35 years a significant decrease in March (month of sea ice maximum) and September (month of sea ice minimum) is obvious as shown in Figure 1.1. The sea ice extent is defined as the area of sea ice concentration bigger than 15 %. This decrease in sea ice extent is related to different large-scale processes, e.g. global warming, changes in incoming radiation and changes in ocean circulation [Serreze et al., 2007], lead to increased sea ice melting due to the positive *ice-albedo-feedback* [Perovich & Richter-Menge, 2009]. Due to higher temperatures sea ice is melting and thus the total Arctic albedo is decreasing. Consequently, more solar heat input is absorbed and the melting enhances. In addition to this, the enhanced melting changes sea ice surface properties determining its reflectivity. Thus, the snow cover is reduced but the fraction of bare ice and melt ponds is increasing immediately. These positive feedbacks are of interest for Earth's climate system as a whole, for they can amplify small regional perturbations to have global impact.

When considering the evolution of sea ice, however, not only sea ice extent is to be studied, but sea ice thickness and age need to be examined. Figure 1.2 illustrates how the fractions of different ice types in the Arctic developed over time whereas the Arctic sea ice today is much younger than 30 years ago (1983: about 45 % multi year ice, 2011: about 25 % multi year ice). Furthermore, it is obvious that ice older than four years disappeared in 2011 almost complete. Particularly drastic is the record minimum in 2007, when the Arctic lost a significant portion of multi year

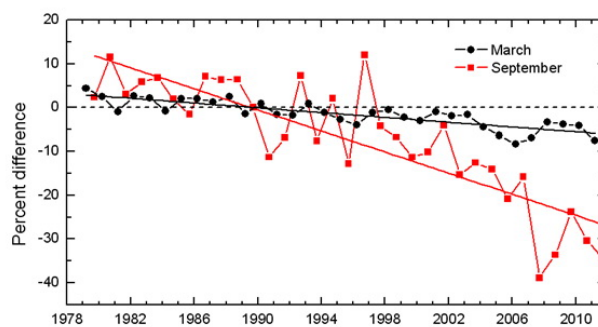


Figure 1.1.: Annual averaged anomalies of the sea ice extent in the Arctic (60° to 90° N) in March (sea ice maximum, black line) and September (sea ice minimum, red line) relative to the period mean from 1979 to 2007 [Richter-Menge et al., 2011].

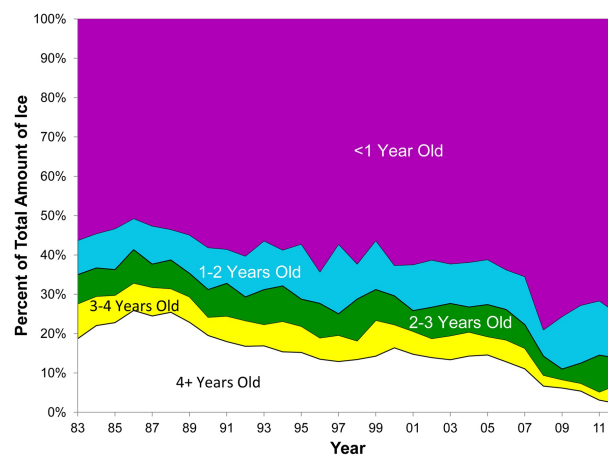


Figure 1.2.: Development of sea ice age from 1983 to 2011. Classification in first year ice (purple) and multi year ice (blue, green, yellow, white) [NSIDC, 2012].

ice. Reasons had been strong ice melting and exporting (through Fram Strait) processes [Smedsrud et al., 2008] as well as strong winds across the Arctic summer and warm air imported from the Pacific connected to higher ice drift velocities [Hakkinen et al., 2008; Kay et al., 2008].

The observed changes of Arctic sea ice over the entire last two to three decades have a strong impact on interactions with the atmosphere and ocean. Due to a more seasonal ice cover the transmitted and absorbed solar shortwave radiation (light) increases significantly. These changes influence sea ice melt as well as biological and geochemical processes in and under Arctic sea ice.

Finally, it is shown that a lot of processes in the coupled system of atmosphere, ocean and sea ice are involved to get an idea of the solar heat input into the ocean and its global impact for all components of the Earth's climate system.

1.3. Background and motivation for this thesis

The preceding sections gave an overview about the importance of sea ice as an boundary layer between the climate system components ocean and atmosphere. It is shown that sea ice has been evolving towards a thinner and younger sea ice cover especially during the last few decades. The decrease in sea ice extent at this point is also mostly reflected in a strong reduction of thick and older sea ice. Thus, the fraction of seasonal sea ice increases resulting in less snow on top of the sea ice, a thinner sea ice layer in general, more trapped salt and a less deformed sea ice cover. Finally, the optical properties of sea ice are affected crucially by these described changes. Major impacts include the reduction of reflectivity towards the

atmosphere and hence an increase in light absorption in the ice layer and an increasing transparency towards the ocean. These components are major factors for feedback processes such as the ice-albedo-feedback (see section 1.2). Consequently, a detailed understanding is highly relevant to modeling the energy budget in polar regions in climate models.

Concerning the reflectivity of sea ice and its changes during the last decades different studies have been set up performed e.g. by Perovich et al. [2002]; Perovich & Polashenski [2012]. These studies give an excellent overview about changes of energy fluxes concerning different kinds of ice types and associated changes in solar heat input into the Arctic Ocean. This raises the question how these changes in surface properties affect the transmittance of sea ice and thus, how radiative fluxes under Arctic sea ice changed during the last decades. In this context, it is not sufficient to understand averaged modifications of radiative fluxes, but rather necessary to gain insights into spatial and temporal variation of solar radiation under different ice types, in order to understand implications for the sea ice mass balance, bottom and basal melting as well as biological and geochemical processes.

The operation of a remotely operated vehicle (ROV) enables metering transmitted light under Arctic sea ice. During the transpolar cruise in 2011 with the German research vessel RV POLARSTERN a ROV has been deployed under mostly snow-free ice of different categories, e.g. varying sea ice age and surface properties (melt ponds/ bare ice). Based thereon, transmittances for first year and multi year ice and in dependence on melt pond fraction have been estimated. This, however, applies to summer conditions only. Additionally, there are not enough and sufficiently well observations of light transmission over larger regions and during different seasons of the year.

In Nicolaus et al. [2012] a first upscaling method for the transmitted light distribution for the entire Arctic has been shown (see Chapter 3.2). Both the summer transmittances for ponded and white first and multi year ice and different satellite and re-analysis products have been used to set up a parametrization of light transmittance through different ice classes which is based on calculations of Perovich et al. [2011] concerning the albedo distribution. This parametrization gives no indication of the seasonality of the transmittance and solar heat input through the Arctic sea ice for an entire year. Accordingly, this thesis is focused on establishing the seasonal dependence of the transmittance of different ice types. Furthermore, the sensibility of sea ice transmittance regarding the influence of timing and length of the melt season has to be verified. These changes are already observed in our days

and will become more and more interesting for the next few years. Consequential effects might be enhanced modifications of the thermohaline circulation and thus, variations in processes concerning sea-ice-air interactions as well as changes related to biological activities in the polar ocean.

Given the initial situation outlined above, the following questions will be covered by this thesis:

1. How much light is transmitted through different kinds of sea ice during different seasons of the year?
2. To what extent has under ice light availability changed over the last decades?
3. How will radiative fluxes through Arctic sea ice be affected by observed and projected climate change phenomena?

2 | Theoretical background

2.1. Optical sea ice properties

Optical properties of sea ice are distinguished into inherent and apparent material properties. Inherent optical properties define the scattering and absorption for snow and sea ice and impurities (material properties). In turn, apparent optical properties depend on both inherent optical properties and the ambient light field (apparent properties) [Briegleb & Light, 2007]. These properties determine mainly the surface energy balance of the Arctic sea ice cover, described in the subsequent section (Section 2.3).

2.1.1. Inherent optical properties

Absorption and scattering by snow and ice determine the spatial and temporal distribution of solar heating in the atmosphere-ice-ocean system.

Absorption in sea ice can be described as the capture of energy or rather light by salt pockets, sediments, soot, algae or enclosed water bubbles. It decreases exponentially with the penetration depth of the radiation in sea ice and is strongly dependent on the radiation flux. The absorbed energy may be re-radiated as heat whereas the measurement follows in terms of the absorption coefficient [Perovich, 1996].

If radiation or energy is deflected from its normal path due to interaction with the matter, this is called **scattering**. Sea ice comprises air bubbles and brine pockets and partially solid impurities. Since the difference between the indices of refraction for these inclusions and the surrounding ice are quite large, the inclusions act as effective scattering centers. Light scattering can be described by the scattering coefficient and the phase function, as long as polarization effects are neglected. The former coefficient describes the energy dissipation from a light beam due to scattering and has the dimension of a cross section. An increased number of scattering centers is associated to a higher scattering coefficient. The phase func-

tion on the other hand describes the angular dependence of energy redistribution by scattering, and can be thought of as a probability density for scattering into a given solid angle interval, when properly normalized. In contrast to the wavelength dependent absorption coefficient of sea ice and brine, both, the scattering coefficient and its phase function can, to leading order, be taken to be constant for light in the visible spectrum. This can be understood to reflect the fact that the scattering structures are much larger than the wavelength of the incident radiation. [Perovich, 1996].

All in all, scattering affects the amount of the given spectrum whereas the absorption entails changes concerning its shape.

2.1.2. Apparent optical properties

The described inherent and microscopic properties result in macroscopic (apparent) optical properties of sea ice. These specify the energy flux and morphology under the Arctic sea ice cover. Apparent optical properties are the albedo and transmittance [Perovich, 1996] which are important for the present thesis and hence explained in the following.

The **albedo** describes the visible reflecting power of a surface. The literature and science distinguishes between spectral and total albedo [Perovich, 1996]. The *spectral albedo* $\alpha(\lambda, t)$ is defined as the ratio of reflected radiation from the surface and the incident radiation whereas both are dependent on the wavelength λ

$$\alpha(\lambda, t) = \frac{E_{u,\lambda}(\lambda, t)}{E_{d,\lambda}(\lambda, t)} \quad (2.1)$$

with $E_{u,\lambda}(\lambda, t)$ upwelling irradiance [Wm^{-2}] and $E_{d,\lambda}(\lambda, t)$ downwelling irradiance [Wm^{-2}].

Since the total solar energy absorbed by the ice and ocean is for sea ice thermodynamic studies often of a big interest, the *total* or *wavelength-integrated albedo* α_t is introduced as

$$\alpha_t = \frac{\int E_{u,\lambda}(\lambda, t) d\lambda}{\int E_{d,\lambda}(\lambda, t) d\lambda}. \quad (2.2)$$

Hence, the total albedo depends on the spectral albedo of the surface as well as on the spectral distribution of the incident radiation. The Arctic sea ice cover is characterized by different surface conditions varying with time and space: i.e. snow-covered ice, bare white ice, melt pond or open water. This variability is also shown in the total albedo values for this region which ranges from 0.06 for open water, 0.15 to 0.4 for ponded ice, 0.77 to 0.87 for snow-covered ice, as shown in

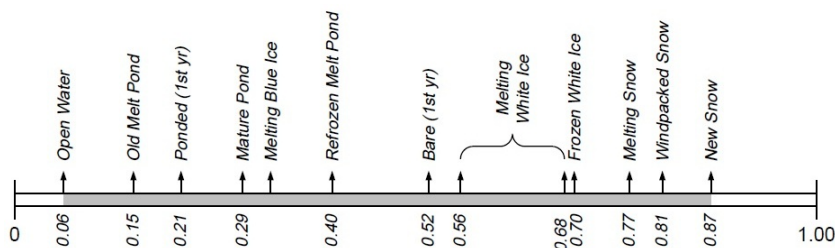


Figure 2.1.: Range of observed values of total albedo for sea ice [Perovich, 1996].

Figure 2.1 [Perovich, 1996].

The light transmission through sea ice is described by the **spectral transmittance** $\tau(\lambda, t)$. It is defined analogously to the albedo as the fraction of the incident irradiance that is transmitted through the ice [Perovich, 1996]

$$\tau(\lambda, t) = \frac{E_{T,\lambda}(\lambda, t)}{E_{d,\lambda}(\lambda, t)} \quad (2.3)$$

with $E_{T,\lambda}(\lambda, t)$: transmitted downwelling irradiance [Wm^{-2}] and $E_{d,\lambda}(\lambda, t)$: surface downwelling irradiance [Wm^{-2}].

Also for the transmittance the wavelength-integrated quantity (*total transmittance*) τ_t suffices for the present treatment

$$\tau_t = \frac{\int E_{T,\lambda}(\lambda, t) d\lambda}{\int E_{d,\lambda}(\lambda, t) d\lambda} = \frac{E_T(t)}{E_d(t)}. \quad (2.4)$$

The spectral distribution of transmitted light through Arctic sea ice is also strongly depended on the surface conditions of the ice cover but also on the physical composition of the ice as well as its thickness. Figure 2.2 gives an overview about the influence of different surface properties on the transmittance of sea ice. The previously described inherent property of scattering seems to have the main impact on the transmittance behavior. It has been shown that optical thick snow due to scattering effects can reduce the transmittance through the ice cover to less than 1%. On the other hand, melting snow as well as the presence of melt ponds decrease the scattering effect and thus increase the transmittance [Perovich, 1996].

2.2. Calculation of radiative fluxes under Arctic sea ice

For the here presented study the total solar heat input through an unit area to the ocean through ice, melt ponds and areas of open water is the sum of the solar heat

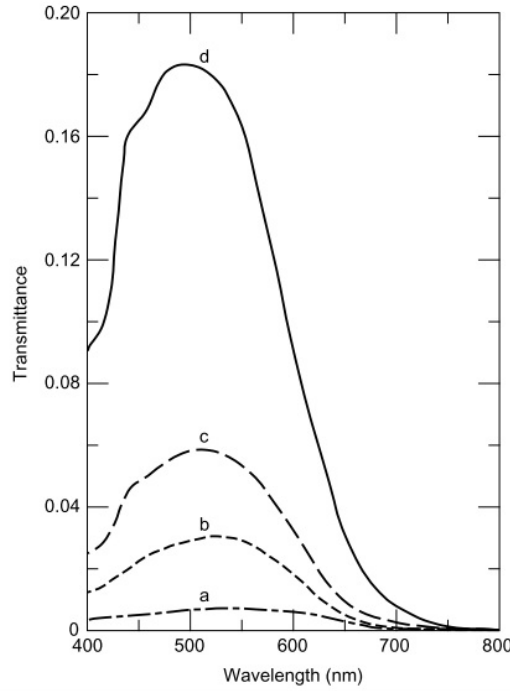


Figure 2.2.: Influence of surface conditions on light transmittance through Arctic sea ice. In all cases the ice thickness was 1.85 m. Surface conditions were a) blue ice covered by 0.25 m of melting snow, b) blue ice covered by 0.12 m of melting snow, c) white ice and d) blue ice covered by a 0.05 m melt pond. [Perovich, 1996].

input through each single component. This can be expressed as follows:

$$E_T(t) = E_i(t) + E_{mp}(t) + E_o(t) \quad (2.5)$$

with E_T : transmitted solar radiation at the bottom of the ice [Wm^{-2}],
 E_i : transmitted solar radiation through white ice [Wm^{-2}],
 E_{mp} : transmitted solar radiation through melt ponds [Wm^{-2}] and
 E_o : transmitted solar radiation through the ocean [Wm^{-2}],
 t : time,

whereas each component is calculated as

$$E_{mp}(t) = E_d(t) \cdot C_i(t) \cdot C_{mp}(t) \cdot \tau_{mp} \quad (2.6)$$

$$\begin{aligned} E_i(t) &= E_d(t) \cdot [C_i(t) - C_i(t) \cdot C_{mp}(t)] \cdot \tau_i \\ &= E_d(t) \cdot C_i(t) \cdot [1 - C_{mp}(t)] \cdot \tau_i \end{aligned} \quad (2.7)$$

$$E_o(t) = E_d(t) \cdot [1 - C_i(t)] \cdot \tau_o, \quad (2.8)$$

with E_d : downwards surface solar radiation [Wm^{-2}],
 C_i : sea ice concentration [m^2m^{-2}],
 C_{mp} : melt pond fraction on sea ice [m^2m^{-2}],
 τ_i : transmittance of ice,
 τ_{mp} : transmittance of melt ponds and
 τ_o : transmittance of open water (ocean), $\tau_o = 0.93$ [Perovich, 1996].

Substituted in equation 2.5, the **solar heat input to the ocean through the entire system including open water** results to

$$\begin{aligned} E_T(t) &= E_d(t) \cdot [C_i(t) - C_i(t) \cdot C_{mp}(t)] \cdot \tau_i \\ &+ E_S(t) \cdot C_i(t) \cdot C_{mp}(t) \cdot \tau_{mp} \\ &+ E_d(t) \cdot [1 - C_i(t)] \cdot \tau_o. \end{aligned} \quad (2.9)$$

For the here presented calculations and studies mostly just the fluxes through the ice and melt ponds excluding the input to the open water are considered. This results in the following equation of the **solar heat input to the ocean through ice and melt ponds**

$$\begin{aligned} E_T(t) &= E_i(t) + E_{mp}(t) + E_o(t) \\ E_T(t) &= E_d(t) \cdot [C_i(t) \cdot (1 - C_{mp}(t))] \cdot \tau_i \\ &+ E_d(t) \cdot C_i(t) \cdot C_{mp}(t) \cdot \tau_{mp}. \end{aligned} \quad (2.10)$$

In the case of no information about the melt pond fraction on the sea ice surface the transmittance of sea ice is set to a mean value of a mixed system of ice and melt ponds, so the solar heat flux results as

$$E_T(t) = E_d(t) \cdot C_i(t) \cdot \tau_{i,s} \quad (2.11)$$

with $\tau_{i,s}$: transmittance of the mixed system of ice and melt ponds.

Arctic-wide sea ice transmittance

Using the equations from above it is possible to estimate the radiation flux (mean, total or modal values) through the Arctic sea ice cover over the entire Arctic as well as the resulting mean transmittance. The mean transmittance of Arctic sea ice is defined as the fraction of solar heat input through Arctic sea ice and the solar heat input over the ice cover (see Section 2.1.2). In the following, the Arctic region

is defined to include latitudes north from 65°N (excluding the pole hole north of 88°N) because that is the region including the main Arctic sea ice extent. The following calculation is valid for both, the transmittance of the system of ice and melt ponds as well as for the entire system including open water areas:

$$\tau_a(i, mp) = \frac{\sum E_T(i, mp)}{\sum E_d(i, mp)} \quad (2.12)$$

$$\tau_a(i, mp, o) = \frac{\sum E_T(i, mp, o)}{\sum E_d(i, mp, o)} \quad (2.13)$$

with τ_a : Arctic-wide transmittance,
 (i, mp) : over/under sea ice and melt ponds and
 (i, mp, o) : over under sea ice, melt ponds and open water.

Daily values of the Arctic sea ice transmittance may then be averaged over time for representative monthly average values of the transmittance behavior of Arctic sea ice.

2.3. Thermodynamics of sea ice - Surface energy budget

The climate system components atmosphere, ocean and sea ice interact directly but also indirectly with each other by means of radiative transfer of energy. The distribution of solar radiative energy throughout the entire system as well as the absorbed and transmitted energy of the sea ice is determined by atmospheric conditions, the sea ice state and the water column below the sea ice cover. Figure 2.3 gives an overview on the important heat fluxes for the surface heat budget of sea ice which are briefly explained in the following.

The surface heat budget for sea ice is composed in general of three types of fluxes: radiative, turbulent and conductive fluxes [Perovich & Richter-Menge, 2009]. The single components of the fluxes for an entire year during 1997/98 are calculated and presented in Huwald et al. [2005] and are quoted in extracts in Table 2.1. Radiative fluxes are the dominant term and are composed of solar radiation (shortwave radiation, spectral range of measured values in this thesis: $\lambda = 250 \text{ Wm}^{-2}$ to 2500 Wm^{-2}) and longwave radiation. The outgoing shortwave radiation is mostly affected by the surface albedo whereas the outgoing longwave radiation is just a function of the surface temperature. However, the incoming longwave radiation is influenced by cloud coverage and is consequently a function of the sky temperature. Depending on the type and altitude of the clouds the consequential decrease of incoming solar

radiation or increase of incoming longwave radiation is the dominant effect. At this point low clouds have a warming effect whereas high clouds tend to cool the surface [Sedlar et al., 2011].

Turbulent fluxes involve sensible and latent heat fluxes. They depend on different atmospheric parameters as wind speed and temperature as well as on the difference in humidity between atmosphere and ocean or ice surface [Perovich & Richter-Menge, 2009].

The last mentioned component of the system is the conductive heat flux. It describes the temperature gradient between two coupled components. The conduction of heat occurs in the ice due to the temperature gradient between the ocean and the atmosphere. It is therefore approximately proportional to the inverse of the ice thickness. Although conductive heat fluxes may occur through a snow cover as well, heat conductivity is significantly reduced in this case [Sedlar et al., 2011].

For a general sign-convention it is determined that downward fluxes are positive and upward fluxes are negative. The sum of all these described fluxes is finally defined as the flux into or out of the ocean. It might be used for phase changes, e.g. ice melting (during summer) or water freezing (during winter), or storage changes, e.g. changes of temperature of sea ice or water [Wendler et al., 1997].

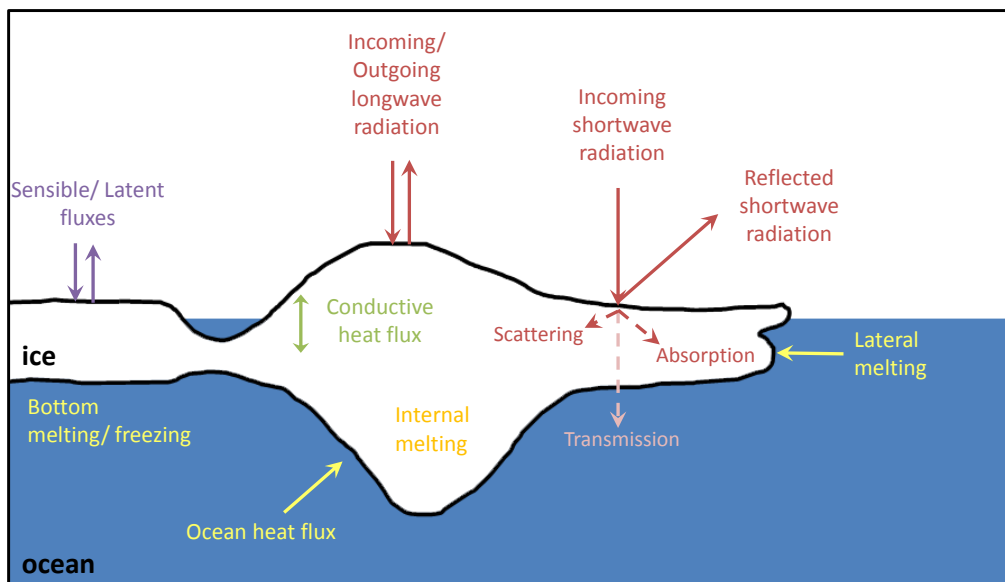


Figure 2.3.: Schematic of the surface heat budget of Arctic sea ice. Purple: Turbulent heat fluxes, red: Radiative heat fluxes, green: Conductive heat flux, yellow: Additionally melting processes. This graphic is based on Perovich & Richter-Menge [2009].

2. Theoretical background

Table 2.1.: Monthly and annual means of the energy budget components from SHEBA field experiment in 1997/98 [Huwald et al., 2005]. The used abbreviations are: F_{swd} , F_{swu} and F_{swp} : downward, upward and penetrating shortwave radiation; F_{lwd} and F_{lwu} : downward and upward longwave radiation; F_{sh} and F_{lh} : sensible and latent heat flux; F_{cs} : conductive heat flux; F_{ocn} : ocean heat flux. All values are given in Wm^{-2} .

Variable	Dec	March	June	Sep	Annual mean
F_{swd}	0.0	46.3	280.4	39.9	92.1
F_{swu}	0.0	-39.4	-200.2	-25.9	-68.5
F_{swp}	0.0	0.6	9.6	0.5	2.9
F_{lwd}	152.0	201.2	282.5	282.2	231.0
F_{lwu}	-185.2	-222.1	-308.2	-293.0	-252.1
F_{sh}	6.4	3.0	1.5	-0.4	2.4
F_{lh}	0.3	-0.6	-2.2	-0.9	-0.6
F_{cs}	19.7	8.3	-2.0	4.6	7.2
F_{ocn}	3.4	7.4	9.9	10.3	7.1

Heat fluxes at the bottom of the ice consists of the heat conduction through the ice and the ocean heat flux from below. Furthermore, melting of the ice cover can also be affected by lateral melting processes at the ice edge [Perovich & Richter-Menge, 2009].

3 | Data and methods

3.1. Data description

In the following, all satellite and reanalysis data sets used for later calculations of the light distribution under Arctic sea ice and its properties are described. These data sets include sea ice concentration, sea ice type, surface solar radiation downwards, melt and freeze onset, and melt pond fraction. All data were interpolated to a 10-km polar stereographic grid. All used data products are also summarized in Table 3.1.

Sea ice concentration

The Ocean and Sea Ice Satellite Application Facilities (OSI SAF) provide, among others, SSM/I (Special Sensor Microwave/Imager) sea ice concentration data (product ID: OSI-401) [Eastwood, 2012]. These sea ice products have been derived from passive microwave, active microwave and optical sensors. The usage of multi sensor methods with a Bayesian approach (inverse method) gives the possibility to combine different instruments and sensors. The SSM/I sea ice concentration is calculated in a first step by following the SSM/I hybrid sea ice concentration algorithm described in Eastwood [2012]. Afterwards, the results are analyzed on the 10-km stereographic grid from OSI SAF.

The developed sea ice concentration is here defined as the areal fraction in percentage with values between 0 and 100% of a given grid cell covered by sea ice [Eastwood, 2012].

The data of the SSM/I sea ice concentration are available from 1979 up to today in two different products: From 1979 to 2008 as reprocessed data sets and from 2006 onwards as operational data sets, both as a multi sensor product. The data sets have systematical differences due to the processing with a different set of tie point statistics for the ice concentration algorithm [Lavergne et al., 2010; Lavergne & Eastwood, 2012]. In our time series analysis, the reprocessed data set used for the years 1979 to 2007, and the operational data set is applied for the subsequent years.

The current 10km Polar stereographic grid is used as basic grid for the whole analysis and so for each included data product.

Surface solar radiation (downwards)

For the downward surface solar radiation the used data are from the global atmospheric reanalysis produced by the European Centre for Medium-Range Weather Forecasts (ECMWF) [Dee et al., 2011]. ERA-Interim is obtained up to four times per day covering the period from 1 January 1979 onwards to 31 October 2012. The solar constant is set to the constant value of 1370 W m^{-2} in European Reanalysis (ERA Interim), hence not including the solar cycle. Variations due to the varying distance between the earth and the sun are, however, incorporated. The horizontal resolution of the downward surface radiation is 1.5° [Dee et al., 2011].

For the following analysis the data sets of 00:00, 06:00, 12:00 and 18:00 UTC were used in the calculation of daily means.

Sea ice age

The spatial distribution of different ice age classes is included through a data product using the algorithm of Maslanik et al. [2007, 2011]. Using satellite data and drifting buoys it is possible to observe different properties of sea ice, like formation, movement, persistence and disappearance of sea ice. The resulting gridded vector fields from 1979 onwards, as a kind of history, describe the basis for the ice age estimate. For this purpose each grid cell that contains ice is treated as a discrete, independent Lagrangian parcel and is then advected at weekly time steps. Resulting, ice that survives the summer melt is appointed to get aged to second year ice and multi year ice is getting an additional year. On the other hand, single grid cells with different ice ages are masked with the age of the oldest particle in this initial method. The final weekly resolved data sets give a determination of nine ice classes (one to nine years or rather older ice) and open water.

For the following analysis the resulting data points with classes of open ocean and ice are set to first year ice, all other data points with mixed values are set to the oldest included age, like in the native method. Furthermore, all ice age data points with a valid value for the sea ice concentration but no valid value for the ice age are set to first year ice. All data points without sea ice concentration data but with ice age values are set to open water.

Melt and freeze onset

Melt and freeze onset dates have been calculated for the entire Arctic using satellite passive microwave data [Markus et al., 2009]. The algorithm makes use of daily averaged brightness temperatures from SSMR and SSM/I mapped on a 25-km polar stereographic grid from the National Snow and Ice Data Center (NSIDC). It distinguishes between the first occurrence of a melt event, the early melt onset (EMO) and the following continuous melt, the melt onset (MO). In this algorithm EMO is defined as the first day of melting independent of the surface temperature, the continuous melt onset as the day after the sea ice stays under melting conditions for the summer. Similar definitions are found for the freeze-up conditions: Early freeze onset (EFO) is the first day freeze-up occurring whereas freeze onset (FO) refers to the day, from which on freezing conditions persist until the next EMO.

The time series of the multichannel passive microwave brightness temperature ranges from 1979 to 2011. This series is composed of three different routines or rather sensor technologies [Markus, 2012]. From 1979 to 2007 the algorithm is based on SSM/I data which have then been adapted to AMSR-E (Advanced Microwave Scanning Radiometer - Earth Observing System) from 2003 to 2010. In 2008 a new adjustment of the routine to use SSM/IS (F17) for the microwave brightness temperatures was developed. Time series analyses are here based on the SSMI data set until 2005, from 2006 to 2010 on the AMSR-E data and on the new adjustment of SSM/IS (F17) afterwards.

Melt pond fraction

The spatial distribution of melt pond fraction on Arctic sea ice can be derived from Moderate Resolution Image Spectroradiometer (MODIS) data of special optical frequency bands (459 to 479 nm, 620 to 670 nm, 841 to 876 nm) in combination with a neural network [Rösel et al., 2011]. The final melt pond fraction results from different typical spectral behavior of melt ponds compared to other surface features like snow, sea ice or open water. Based on this, an artificial neural network was built and trained according to the method of Tschudi et al. [2008]. After validation of the resulting melt pond fractions with different local observation products, the data set is scaled with the sea ice concentration from the NSIDC to obtain the relative melt pond fraction.

The spatial cover extends from 60 to 90°N with mean values of 8-day intervals beginning on 9 May to 13 September each year (2000 to 2011).

Melt onset and melt pond fraction data sets appear to contradict each other. In

Table 3.1.: Description of all used data sets for later analyses. The data sets were interpolated to a 10-km polar stereographic grid.

Data set	Source	Available period	Used period
Surface solar radiation downwards	ECMWF	1979-2012 (daily)	1979-2012
Sea ice concentration	Ocean and Sea Ice SAF (OSI SAF)	reproc. 1979-2009; operat. 2006-today (daily)	reproc. 1979-2007; operat. 2008-today
Sea ice type/age	Maslanik et al. [2007]	1979-today (weekly)	1979-today
Melt/Freeze onset	Markus et al. [2009]	SSMR 1979-2007; AMSR-E 2003-2010; SSM/IS 2008-2011 (annual)	SSMR 1979-2005; AMSR-E 2005-2010; SSM/IS 2011
Melt pond fraction	Integrated Climate Data Center (ICDC)	2000-2011 (09.05.-13.09., 8-day-mean)	2000-2011

some cases, the derived melt pond fraction is non-vanishing, although, according to the melt onset data, melting has not yet begun. Then, the melt onset data are supposedly more reliable. Thus, melt pond fractions before EMO are set to zero.

For the application of all described data sets and the following calculations the effect of ice drifting is neglected. Sea ice drift is mostly effecting the edge of the sea ice area. With the given data sets it is not possible to involve these effects.

3.2. Calculation of light transmission through Arctic sea ice during August 2011

Based on available large-scale under-ice light measurements carried out in August 2011 [Nicolaus et al., 2012, 2013], estimates of light availability under sea-ice during summer spanning the whole Arctic can be given. The respective method is briefly presented in the following.

During the transpolar cruise ARK-XXVI/3 (TransArc) with the German Research Vessel POLARSTERN in summer 2011 (August to October) measurements of radia-

tive fluxes under Arctic sea ice with different surface properties, e.g. melt ponds or bare ice, have been performed. These measurements were based on two Ramses spectral radiometers (320 to 950 nm) operated under the Arctic sea ice on a Remotely Operated Vehicle (ROV) [Nicolaus & Katlein, 2013]. The irradiance sensor measures the incoming energy throughout the (upper) half space to resolve basal melt and biological processes and hence, give a better understanding of the energy budget of the sea ice cover and the total fluxes. The radiance sensor has a narrow field of view (7°) and thus enables deriving of optical properties with higher spatial resolution. The measurements of both sensors covers a wide range of light conditions under the central Arctic sea ice cover. In addition, incident solar radiation was measured synchronously on the sea-ice surface. The combination of these measurements enables the calculation of transmittances of the sea ice for the region.

The shortwave transmittances of first year ice (19 August 2011) and multi year ice (22 August 2011) calculated from the measurements directly under the sea ice cover are plotted as frequency distributions in Figure 3.1. In combination with observation of sea ice type, snow depth and pond coverage it is possible to assign four modes to specific ice classes, tagged in Figure 3.1. The mode of 0.01 can be assigned to white MYI whereas the transmittances of white FYI amount around 0.04. For ponded ice the derived mode of FYI is between 0.18 to 0.22 and for MYI between 0.12 and 0.14 [Nicolaus et al., 2012]. Due to different ice thicknesses and snow coverage the modes are quite elongated and overlap mutually.

However, the given data set of field measurements only covers the spectral range of the Ramses radiometers from 320 to 950 nm [Nicolaus et al., 2010b]. In comparison

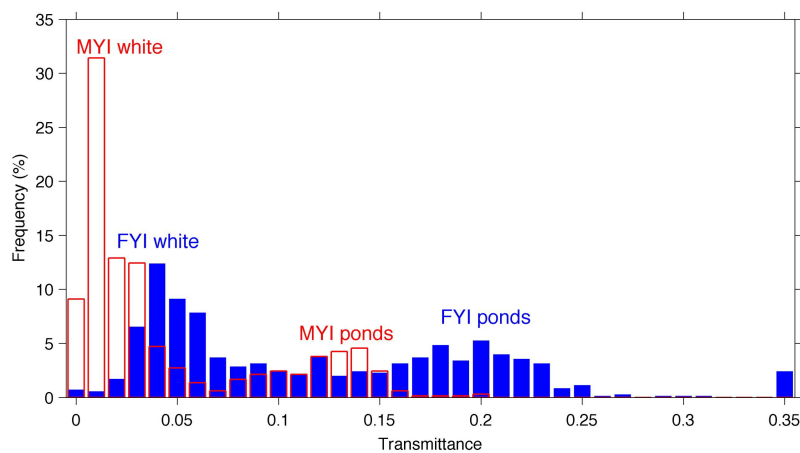


Figure 3.1.: Histogram of transmittances measured during TransArc 2011 [Katlein, 2012, modified]. Clearly detected modes for first year ice, multi year ice and melt ponds in general are marked.

3. Data and methods

with the reference spectra following Grenfell & Perovich [1984], the spectral range of the Ramses radiometer covers on average only 79.51 % of the total irradiance [Nicolaus et al., 2012]. Finally, all under-ice radiation data sets were scaled to the entire range of shortwave radiation from 250 to 2500 nm. This results in values of modal transmittance through ponded and white first year and multi year ice shown in Table 3.2.

In addition, during the cruise sea ice observations from the bridge have been performed throughout the cruise. These observations lead to a melt pond fraction of $(42 \pm 10) \%$ on FYI and $(23 \pm 13) \%$ on MYI. To estimate the total transmittance for FYI and MYI, it is necessary to include these different fractions of ponded and white ice for both ice types. The resulting total transmittances for summer conditions for this distinction are 0.11 for FYI and more than a third from this with 0.04 for MYI [Nicolaus et al., 2012].

Based on these total transmittances for FYI and MYI obtained by field measurements in combination with additional data sets of sea ice concentration, sea ice types and surface solar radiation (see Chapter 3.1) an Arctic-wide estimate of light transmission through Arctic sea ice in August 2011 is possible. That estimate is

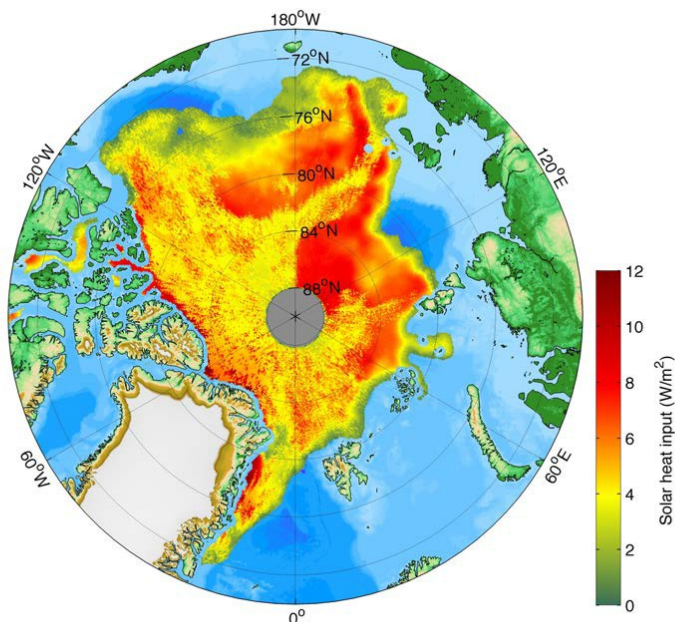


Figure 3.2.: *Solar heat input into the Arctic Ocean through sea ice. This map only consider fluxes through sea ice, excluding fluxes through open water, for August 2011 [Nicolaus et al., 2012].*

Table 3.2.: Measured and calculated transmittances during summer (no snow) of first year and multi year ice subdivided in white ice, melt ponds and the entire system of both components. The total transmittances result from the TransArc 2011 experiment, the ICDC transmittances are calculated with there given melt pond fraction. The last column represents the transmittances which are used in the following calculations.

				ship observations		ICDC data set	
Ice type		modal transmittance	melt pond fraction	total transmittance	melt pond fraction	total transmittance	
FYI	white	0.04	$(42 \pm 10) \%$	0.11	26 %	0.087	
	ponded	0.22					
MYI	white	0.01	$(23 \pm 13) \%$	0.04	29 %	0.05	
	ponded	0.15					

following Equation 2.11 calculated for each grid cell and each day and subsequently, monthly averaged. The resulting heat input through the Arctic sea ice into the upper Arctic ocean (excluding fluxes through open water) amount to values between 0 and 13 W/m^2 . The distribution of the heat flux through sea ice is shown in Figure 3.2.

That estimate is valid just in case of no snow cover on top of the sea ice surface and open and fully developed melt ponds assumed for August 2011.

3.3. Newly developed method for seasonality of transmittance

The estimate of the Arctic-wide transmitted light distribution under sea ice described in Nicolaus et al. [2012] covers summer sea ice conditions only. To get an idea of the seasonal cycle of the transmittance of Arctic sea ice additional data sets and assumptions have to be involved. That implies an improved ice type classification including the spatial distribution of melt ponds and the dates of melt and freeze onsets as well as the duration of the melt and freeze phase. Furthermore, a spatial distribution of melt ponds based on satellite data is included.

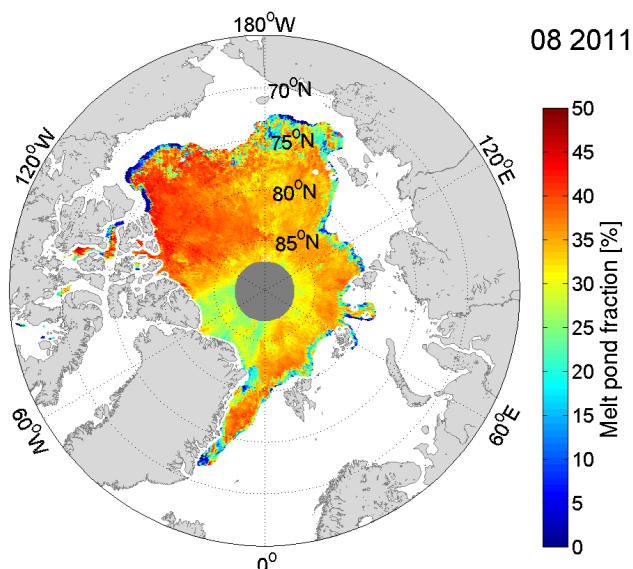


Figure 3.3.: Mean melt pond fraction in August 2011 [Rösel et al., 2011].

3.3.1. Improved spatial distribution of melt ponds

An algorithm to estimate the fraction of melt ponds on both, first year ice and multi year ice, has been proposed in the literature [Rösel et al., 2011]. The approach relies on data provided by the Integrated Climate Data Center (ICDC). Some sample output showing the melt pond fraction in August 2011 is given in Figure 3.3. That data set gives a lower melt pond fraction on FYI than the observed fraction from the ship during TransArc 2011 (26 %) but a higher one for MYI (29 %). Within the error margins both values seem to be almost identical, so the difference between the melt pond fraction on FYI and MYI is negligible. The resulting values for the total transmittance with these changed melt pond fraction differ in a similar way, so it is now 0.087 for FYI and 0.05 for MYI.

Since the ICDC data sets enables the application of a spatial distribution of the melt pond fraction in contrast to the generalized observed distribution, the data set is used for the following analysis. Furthermore, the data set is validated with different kinds of local observations done by ship or plane.

All measured and calculated results are valid only for summer conditions, this means without snow on the top of the sea ice cover, are summarized in Table 3.2.

3.3.2. Ice type classification

Using sea ice age data to divide the sea ice surface into different categories allows to include a lot of optical properties via one data set. The sea ice age implies in that process information and estimates about the sea ice thickness, roughness and deformation of the sea ice surface. These characteristics are crucial for optical properties of sea ice, thus giving an important basis for the development of the seasonal transmittance of Arctic sea ice.

The initial classification of sea ice is based on ice age categories from 1 to 10 years and open water Maslanik et al. [2007]. For the following processing this categorization is eliminated since ice older one year yields comparable optical properties. Thus, this categorization is reduced to first year ice (FYI) and multi year ice (MYI) which includes all ice classes older than 1 year. That simplification has also been used in the preceding estimate of Arctic-wide summer transmittance.

In order to obtain an improved parametrization of the transition from winter to summer time it is necessary to introduce more detailed ice class during that period. Based on this detailed classification the seasonality of the transmittance of Arctic sea ice can be developed, described in Chapter 3.3.5. The extended ice type classification is illustrated in Figure 3.5 (Chapter 3.3.4) related to the annual cycle of sea ice surface properties.

During summer, parts of both FYI and MYI melt and pass over to open water. Therefore, it is necessary for each grid cell, which is containing ice, to calculate at what point in time the respective cell is getting free of ice. In order to neglect the influence of ice drift the day of ice cover disappearing is calculated the other way around: Starting at the end of the melt season (scheduled at the 7 September 2011) each grid cell is monitored until the first time sea ice is appearing. This day is then recorded as the last day of the melt season for this grid cell. The first day of the melt season is the same for the entire Arctic and is calculated as the spatial average of the early melt onset. For 2011 it this was the 139th day of the year (15 May 2011) [Markus et al., 2009]. These new ice categories can be summarized as *melting FYI* and *melting MYI*.

Furthermore, the shift from FYI to MYI after the summer melt has to be included: Sea ice particles of first year ice which survived the summer melt and still exist around week 36/37 of the year are now called multi year ice and are masked like this in the data set of Maslanik et al. [2007]. The immediate change of sea ice properties associated with this tagging is of course not actually observed. Hence,

in the analysis, new MYI is treated as FYI up to the winter period, and only then promoted to real MYI. During the MYI formation period, it is labeled as *new multi year ice*.

A similar procedure is developed for new first year ice growing after the summer melt. Also in this case an instantaneous change from open ocean to ice covered data points occurs. Thus, all grid points with newly formed ice after the shift from FYI to MYI (after the melt season) are classified as 'new first year ice'.

3.3.3. Melt and freeze phases

To embed the different described ice classes in the course of the year, the year is divided based on characteristic melting and freezing days. These days are the early melt onset (first day of observed melting conditions) and melt onset (first day after continuous melting conditions) as well as the early freeze onset (first day of observed freezing conditions) and the freeze onset (first day after continuous freeze-up) [Markus et al., 2009]. For the year 2011 these characteristics are illustrated in figure 3.4. For the spatial average values result for the EMO the 139th day of the year (15 May 2011), the MO the 150th day (30 May 2011), the EFO the

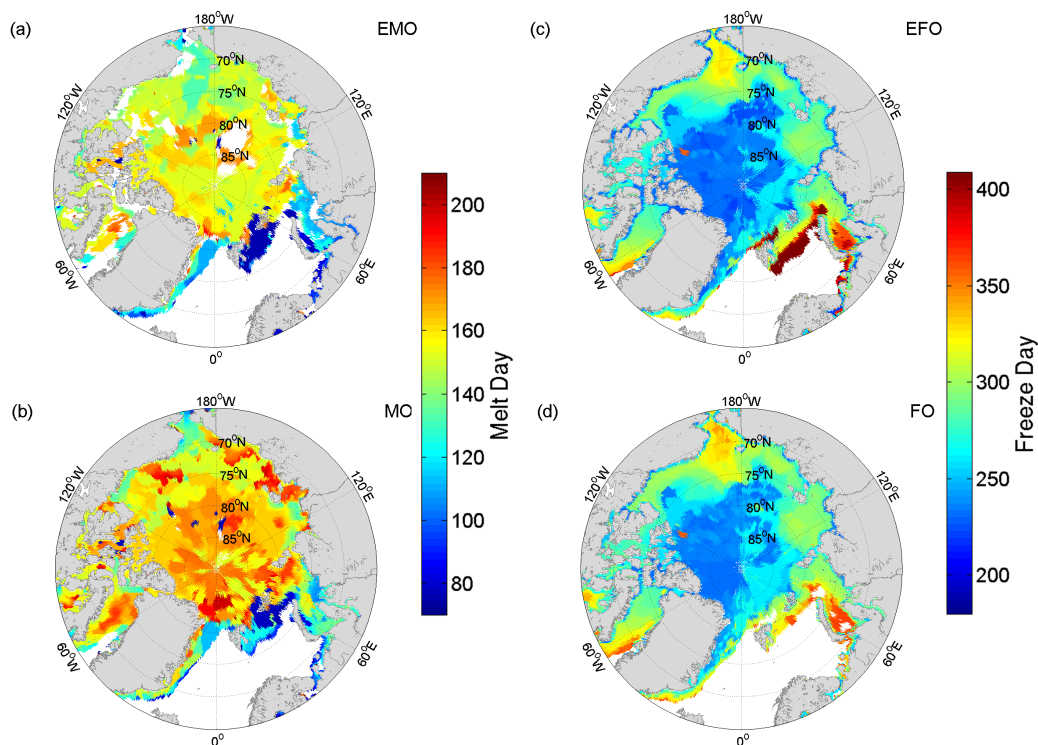


Figure 3.4.: Characteristic melting and freezing days as day of the year in 2011 [Markus et al., 2009]. (a) Early melt onset (EMO), (b) Melt onset (MO), (c) Early freeze onset (EFO), (d) Freeze onset (FO).

280th day (7 October 2011) and the FO the 285th day of the year (12 October 2011).

In addition, the duration of the melting phase and by association the phase classifications are determined by using different studies and experiments. During the Surface Heat Budget of the Arctic Ocean (SHEBA) drift experiments [Perovich et al., 2002] a melt phase duration of about 16 days was derived for MYI. By dividing the data in comparable phases like for the SHEBA data, Nicolaus et al. [2010a] obtained for the TARA drift a melting phase duration of 12 days. For the albedo evolution of seasonal Arctic sea ice several field experiments near Barrow Alaska were done [Perovich & Polashenski, 2012]. The evolution sequence in this case is dominated by the SHEBA onset data as well and gives a resulting melt duration of 14 days for FYI.

Summarizing these values from different experiments a general melting phase duration of 14 days is derived for the following seasonal studies of Arctic sea ice properties. This phase is beginning at the date of the melt onset.

For the specification of the duration of the freezing period no references are available since no conclusive experiments at winter time have been carried out to date. Due to this fact the phase duration is committed to a value of 60 days beginning at the freeze onset.

3.3.4. Sea ice surface properties

For the development of the seasonality of the Arctic sea ice transmittance it is necessary to divide the whole year into an amount of different phases. These phases are described in the following using the sea ice observations from the Arctic Transpolar Drift in 2007 (Tara) [Nicolaus et al., 2010a] and the SHEBA field experiment (1997-1998) [Perovich, 2005]. The given distinctions between the phases are given for simplifications as fixed and clear dates. In reality the transition between the phases is not that obvious because of permanent changes in surface conditions. The development of the surface properties is in addition illustrated in figure 3.5.

Phase I (winter) is the phase of winter conditions. That can be described by a closed ice cover without any melt ponds but with partly snow on top. A cold, dry and optically thick snow layer is the defining characteristic. Thus, radiative fluxes under the sea ice cover related to transmitted light are negligible. Furthermore, the temperatures are well below the freezing point. For the analysis this phase is finished when the first melt is observed, i.e. the day of the first occurrence of melting conditions (EMO, see section 3.1).

Phase II (snow melting/spring) describes the occurrence of first melting. For this

part of the year the snow thickness starts to decrease and the temperature of the surface and the ice increases. Consequently, the snow cover melts on parts of the ice cover largely and water deposits can be observed. This phase ends explicit when the conditions of first melting pass over into continuous melting (MO).

Phase III (pond formation/ continuous melting), the time of continuous melting, lasts 14 days beginning from the first day of continuous melting. During this time the snow cover is disappearing completely and the melt pond coverage increases

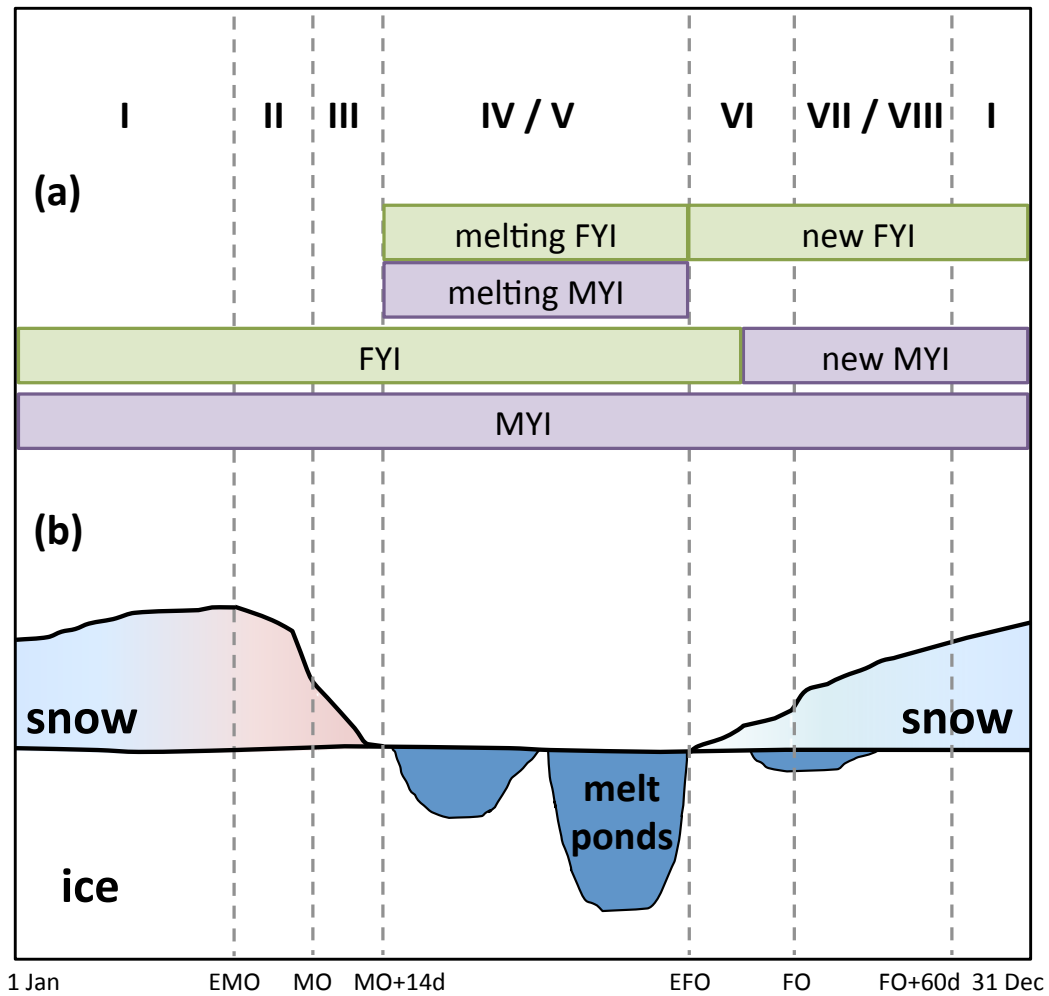


Figure 3.5.: (a) Extended ice type classification of FYI and MYI. (b) Annual cycle and development of the surface properties of Arctic sea ice. The change of ice thickness during the year is neglected. Indicated phases: I: winter, II: snow melting, III: pond formation/ continuous melting, IV: pond evolution/ summer, V: sea ice melting, VI: fall freeze-up, VII: continuous freezing, VIII: new ice growth. This plot is based on sea ice property descriptions in Nicolaus et al. [2010a]; Perovich et al. [2002].

rapidly up to 15 to 20%. Accordingly the sea ice surface gets more and more covered with water deposits which can not drain. Completed snow melting marks the end of this phase.

Phase IV and V (pond evolution/ summer) is mainly characterized by accumulating of the growth and areal extent of the melt ponds as well as a general surface drainage. For a more precise characterization and study of this phase, it is separated into two parts: *Phase IV* includes the part of the ice which is completely melting during the summer time whereas *phase V* qualifies the first and multi year ice surviving the summer melt. The main defining property for this phase is the snow-free surface which is covered more and more with melt ponds. With the first occurrence of freeze-up conditions this summer phase is over.

Phase VI (fall freeze-up) is beginning with the day of early melt onset which determines a sharp shift from summer to first freezing conditions. During this time air and surface temperatures drop below 0 °C resulting in first surface freezing and snow accumulation. Nevertheless, former melt ponds are still visible through the new snow cover. Sea ice that survived the summer melt is promoted to one year older ice in week 37/38 according to Maslanik et al. [2007]. However, first year ice shifting to multi year ice remains first year ice regarding its optical properties until the end of the year (see section 3.3.2). Beginning with the first day of continuous freeze-up this phase is ending.

Phase VII (continuous freezing) for the new and 'old' multi year ice covers following the entire freezing period of 60 days beginning with the continuous freeze-up onset. Prominent changes regarding the surface properties in this phase include an increasing snow depth and the gradual disappearance of melting ponds up to the point of full snow and ice cover.

Phase VIII new ice growth can be observed concurrently with phase VI and VII. This new ice is initially growing up very fast. The reason for this is that thin ice is able to conduct much more heat from the ocean to the atmosphere than thicker ice. Consequentially, the ice growth rate is comparatively high. At the end of the freezing phase, so 60 days after the first day of continuous freezing, the properties of all types of newly formed first year ice can be considered as equivalent.

The subsequent part of the year is again characterized by an entire closed snow and ice cover. Thus it is also described as phase I (*winter*).

3.3.5. Development of seasonal transmittance of Arctic sea ice

Transmittance of the entire system of ice, snow and melt ponds

The preceding section describes the main variances of the sea ice surface over the year. These properties and changes are crucial for the physical and optical properties of sea ice, such as absorption, reflection and transmittance. As for the radiation budget under the sea ice surface the transmittance has the largest impact, and its variation during the outlined phases will be derived in the following. All subsequently declared and discussed transmittances exclude the measured influence of biological activity like algae light absorption [Perovich et al., 1998]. The described values of transmittance in the following are for the entire system of ice, snow, melt ponds and open water, if the melt pond data set of the Integrated Climate Data Center (ICDC, see section 3.1) does not provide reliable data, e.g. for areas of too high cloud coverage. Also for the time before 2000, when in general no information about the melt pond fraction is available, these averaged transmittances are used.

Figure 3.6 illustrates the transmittance's evolution with time for an entire year. It's values during the different phases are tabulated in Table 3.3.

Reference points for the development of the transmittance of Arctic sea ice are again observations and measurements done during the SHEBA experiments [Perovich, 2005] and the Arctic Transpolar drift in 2007 (Tara) [Nicolaus et al., 2010a] as well as analyses from previous observational data sets of optical sea ice properties done by Perovich [1996], Perovich et al. [1998] and Nicolaus et al. [2010b]. The main input for the **summer** season (*phase V*), i.e. the phase of no snow and melt ponds on the sea ice surface, are the calculated transmittance data from section 3.2, summarized in table 3.2. At this point not the values obtained during TransArc 2011 are used but the ones calculated with changed melt pond fraction based on Rösel et al. [2011]. Hence, the used value for transmittance of FYI is 0.087 and 0.05 for MYI. Comparing these values to the measurements of the Arctic Transpolar drift in 2007 clear abnormalities are significantly because of strong influences of biological activity [Nicolaus et al., 2010a]. However, when comparing the albedo values of both campaigns, the values are almost identical and in both cases constant for the entire period. Thus, it is justified to estimate a constant summer transmittance.

During the first and last phase, called **winter**, the characterization of the optical properties of sea ice based on measurements is not that obvious because of a very small solar elevation angle and principally few available data sets. During the Tara Drift first measurements were done during formal spring conditions but ice con-

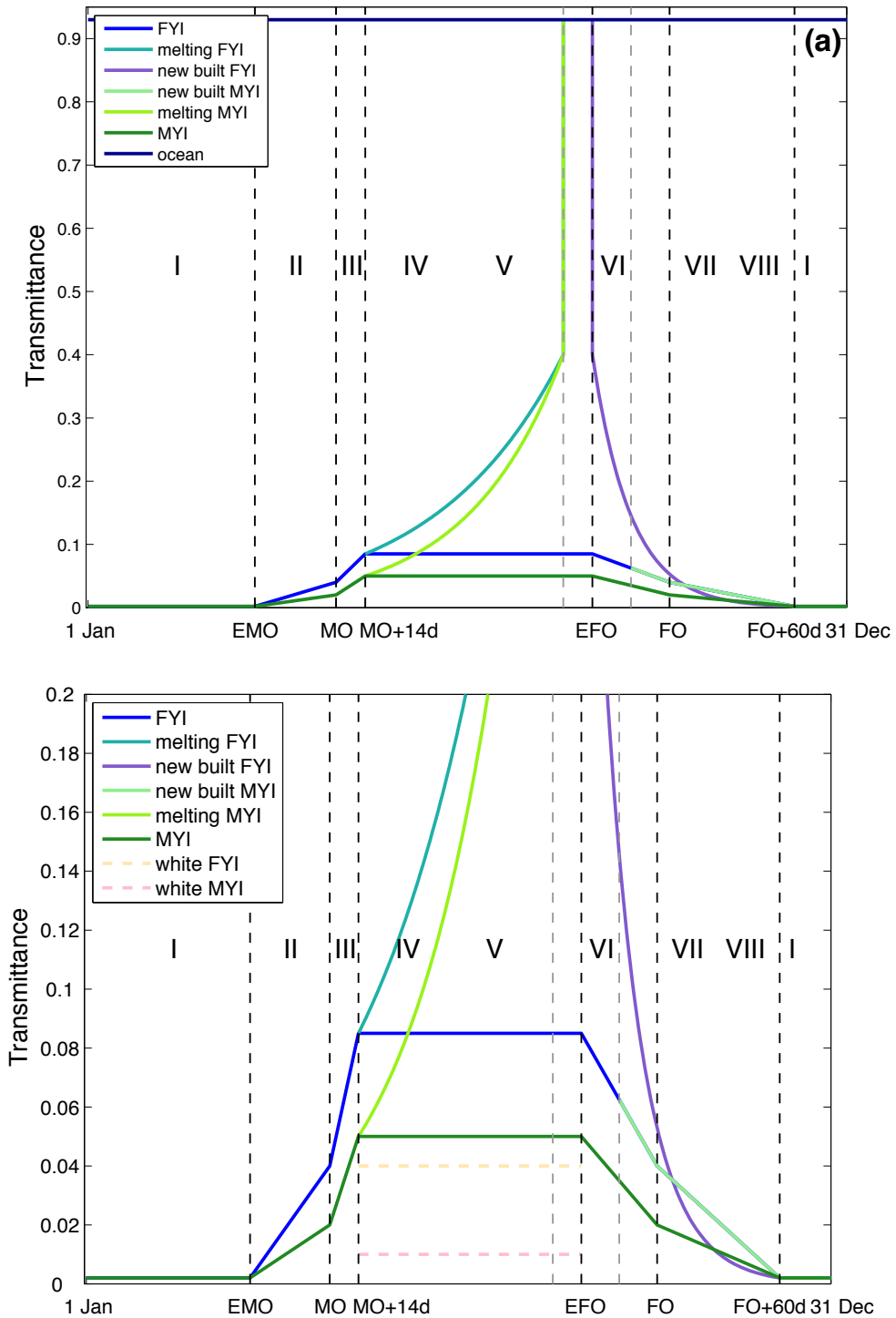


Figure 3.6.: Progress of the transmittance of Arctic sea ice for the entire system of ice, snow and melt ponds. The indicated phases are similar to figure 3.5. (a) The entire range up to transmittances of 0.95. (b) Zoom on in the lower part up to a transmittance of 0.2.

ditions were still comparable to winter conditions. Thus, the ice was covered by an optically thick layer of snow (up to 0.64m) and no melt ponds are visible. For this condition calculations of transmittances of multi year ice were resulting in an average value of 0.002 (averaged over 42 days from 29 April to 9 June) [Nicolaus et al., 2010a]. Assuming the snow cover to be optically thick on both FYI and MYI, independent of the sea ice thickness below, FYI transmittance is expected to be same as for MYI. Comparable values are given in Perovich [2005] (less than 10^{-3}).

Also for the following melting phases the results of the Tara experiments give the main input. A significant increase in transmittances up to 0.02 for MYI, starting with the **snow melting** (*phase II*), lasting to the end of phase II, is apparent. At this point it reaches for MYI a value of 0.02. With the end of this snow melting phase a new development of the transmittance is obviously noticeable by a stronger gradient (*phase III, pond formation*) until the beginning of the summer [Nicolaus et al., 2010a]. Both, the increase during *phase II* from EMO to MO as well as the subsequent increase during the melting phase of 14 days can be considered simply

Table 3.3.: Declared and discussed transmittances subdivided in first year ice (FYI) and multi year ice (MYI) for the entire system of ice and melt ponds, the particular components ice/snow and melt ponds as well as the open ocean. The significant days for dividing the year in different phases are: Early melt onset (EMO), melt onset (MO), melt onset plus melting phase (MO+14d), early freeze onset (EFO), threshold ice-ocean, freeze onset (FO) and freeze onset plus freezing phase (FO+60d).

	winter (until EMO)	MO	summer (MO+14d to EFO)	threshold ice-ocean	FO	threshold ocean-ice	winter (from FO+60d)
FYI, system	0.002	0.04	0.087	0.4	0.04	0.4	0.002
MYI, system	0.002	0.02	0.05	0.4	0.02	0.4	0.002
FYI, ice/snow	0.001	0.017	0.04	0.17	0.017	0.17	0.001
FYI, melt pond	0.15						
MYI, ice/snow	0.0	0.004	0.01	0.07	0.004	0.07	0.0
MYI, melt pond	0.22						
open ocean	0.93						

as linear between the distinctions. The optical behavior for FYI can be considered comparable to the described one of MYI with the main difference of an in general stronger increase due to thinner ice. Looking at the seasonal cycle of the albedo of the Arctic sea ice surface, developed by Perovich & Polashenski [2012], this difference between both ice types also becomes apparent. For the whole transition time an averaged factor of about 2 between both ice types can be identified. Thus, this factor of 2 is transferred to the transmittance of first year ice. As a result, a transmittance value of 0.04 for the transition from phase II to phase III (so the first day of continuous melting, MO) for first year ice is obtained.

As soon as the summer period is finished, a new layer of snow is formed and temperature is decreasing, total transmittance is starting to decrease rapidly (**fall freeze-up**). Comparing the data for this *phase VI* of the Arctic Transpolar drift with the inverse phase III, described before, a similar behavior is found [Nicolaus et al., 2010a]. Accordingly, the temporal progress for the freezing phases can be adjusted to the one of the melting phases. The boundary value between the fall freeze-up and the continuous freezing, specified as the the first day of continuous freezing conditions, as it is also assumed 0.04 for first year ice and 0.02 for multi year ice. The gradient for the following **continuous freezing** phase of 60 days is weaker because of the longer duration of this phase. The last value for this decrease is again the value of the respective transmittance for first year or multi year ice. Linear approximation yields a sufficiently well description of the time evolution during both freezing phases.

The seasonality of the transmittance for completely melting Arctic sea ice as well as for newly formed sea ice must be considered independently of the previously described consisting sea ice. The main question in this case is how the transmittance during the transition from open water to ice, and vice versa, changes. Thus, it is important to decide up to which value the transmittance may initially rise before the properties of melting ice pass over to open water. This value is called **phase transition threshold** in the following. Assuming that for the process of new ice formation the behavior of the albedo with the one of the transmittance is equal, it is possible to draw the following conclusion:

Perovich [1996] presents laboratory observations of initial ice growth experiments with integrated measurements of the spectral albedo during the ice growth. Up to a thickness of 5 cm, the albedo only increases negligibly. During the next 2.5 cm in turn increases considerably. That is indicated in a jump from an albedo value of 0.11 for 5 cm to 0.26 for 7.5 cm. Consequently, the factor for the transition in albedo values results in about 2.36. Applying this factor now also at the phase

transition of the transmittance of open water ($\tau_o = 0.93$) to a thin sea ice layer of just a few centimeters, a threshold of about 0.39 is obtained. As already described before, for the whole process of calculations and analyses, ice is just detected as ice if the amount of the ice cover for the concerned grid cell is bigger than 15 %. This implicates that these detected ice cells have in most cases already a not negligible ice thickness at the point of their first occurrence. Therefore, it is realistic to shift the transmittance from open water ($\tau_o = 0.93$) directly to the transmittance value of $\tau_i = 0.4$ for an ice layer thickness of 7.5 cm. The same threshold is assumed for the progress vice versa, i.e. from melting Arctic sea ice to conditions of open water.

Melting first and multi year ice (*phase IV*) can be treated in the same way as ice surviving summer until the beginning of the summer period. With the beginning of the summer phase until the phase transition threshold of 0.4 (the disappearance of the ice cover) a rapid increase in the transmittance of first and multi year ice is adopted. This increase in transmittance is described in Perovich [1996] as roughly exponentially and is therefor characterized by the following equations:

The general equation for exponential behavior

$$\tau(t) = \tau_0 \cdot k^t \quad (3.1)$$

becomes with insertion of the supporting points of the beginning of the summer (MO plus 14 days) and the point of the phase transition to

$$\tau(t) = \tau_{th} \cdot \left(\frac{\tau_{th}}{\tau_{sum}} \right)^{\frac{t_{MO}-t}{t_{th}-t_{MO}}} \quad (3.2)$$

with t : time in days,
 $\tau(t)$: transmittance at the time of t ,
 t_{MO} : melt onset plus 14 days in days,
 τ_{sum} : transmittance of summer phase: FYI: 0.087, MYI: 0.05,
 t_{th} : day of phase transition threshold in days and
 τ_{th} : transmittance of phase transition threshold: $T_y = 0.4$.

Transmittance of **new first year ice** evolves correspondingly to the melting sea ice surface (*phase VIII*). From the first day of new ice occurrence until the end of the continuous freezing phase (the day of continuous freezing plus 60 days) the strong growth in ice thickness involves a roughly exponential increase in light transmission through the Arctic sea ice. In this case the general exponential function 3.1 is converted to

$$\tau(t) = \tau_{th} \cdot \left(\frac{\tau_{th}}{\tau_{win}} \right)^{\frac{t_{FO}-t}{t_{th}-t_{FO}}} \quad (3.3)$$

with t : time in days,
 $\tau(t)$: transmittance at the time of t ,
 t_{FO} : freeze onset plus 60 days in days,
 τ_{win} : transmittance of winter phase of FYI : 0.002,
 t_{th} : day of phase transition threshold in days and
 τ_{th} : transmittance of phase transition threshold: $T_y = 0.4$.

When the freezing phase is finished, the new first year ice behaves in its properties like the first year ice in the beginning of the year and stays at the transmittance value of 0.003 for the remaining **winter time** (*phase IX*).

With these described phases it is now possible to parametrize the annual cycle of the transmittance of Arctic sea ice for an entire year. The described system is composed of the components ice, snow and melt ponds.

Transmittance of the subdivided system of ice/snow and melt ponds

For grid cells including information about the melt pond fraction the described system can be subdivided into (1) ice and snow fraction and (2) melt pond fraction. Due to no nuanced data sets about radiation fluxes under different melt pond formations or different optical properties, the transmittance of the **pure melt pond** data sets is not subject to any annual cycle but rather constant. Thus, it is set to the determined modal transmittance of 0.22 for melt ponds on first year ice and 0.15 on multi year ice, measured during the Transpolar Cruise in summer 2011 (see table 3.2).

The transmittance of the part of the Arctic sea ice area covered by **bare ice** should again have an annual cycle. This one is also dominated by the optical properties of sea ice during one year described in section 3.3.4. For the transmittance during the summer season of white ice, it is also possible to make use of the measured transmittance at the Transpolar Cruise 2011 with the values of 0.04 for white first year ice and 0.01 for white multi year ice. For the remaining time, a qualitative similar annual cycle is assumed as for the transmittance of the entire system of ice, snow and melt ponds, developed in the subsection before. The quantitative difference between both system is described by the ratio of the established transmittances of the summer season for the entire system and for the white ice. This transmittance

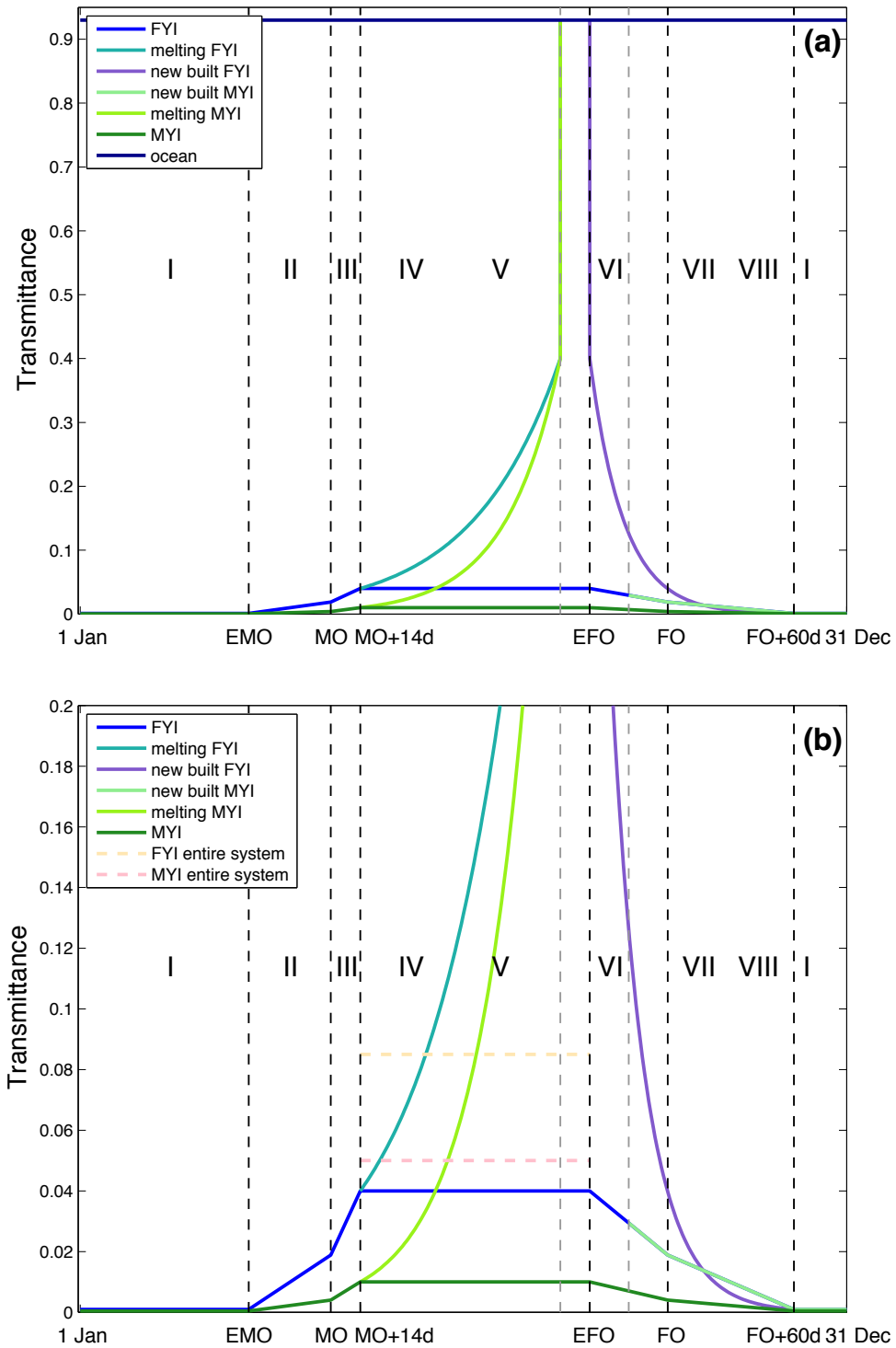


Figure 3.7.: Progress of the transmittance of Arctic sea ice for the bare ice without melt ponds. The indicated phases are similar to figure 3.5. (a) The entire range up to transmittances of 0.95. (b) Zoom in in the lower part up to a transmittance of 0.2.

of pure white ice including the introduced ratio is calculated as follows

$$\tau_i(t) = \tau_s(t) \cdot \frac{\tau_{i,s}}{\tau_{s,s}} \quad (3.4)$$

with $\tau_i(t)$: transmittance of bare ice at the time of t,
 $\tau_s(t)$: transmittance of the entire system at the time of t,
 $\tau_{i,s}$: transmittance of bare ice during summer:
 $\tau_{i,s}(FYI) = 0.04$, $\tau_{i,s}(MYI) = 0.01$ and
 $\tau_{s,s}$: transmittance of the entire system during summer:
 $\tau_{s,s}(FYI) = 0.087$, $\tau_{s,s}(MYI) = 0.05$.

The only exception for this ratio multiplication is the case of the phase transition threshold. This value is also for bare ice fixed at the value of 0.4.

The so obtained annual cycle of pure first year and pure multi year ice is illustrated in figure 3.7 and is subdivided into the different phases in table 3.3.

The described temporal progresses of the transmittance of Arctic sea ice for the entire system of sea ice, snow and melt ponds as well as for the subdivided components of sea ice and melt ponds provides the basis for the subsequent calculation of radiative fluxes under Arctic sea ice during an entire year.

4 | Results

4.1. Light distribution under Arctic sea ice during August 2011

Nicolaus et al. [2012] present a first estimate of Arctic-wide light distribution under sea ice based on a simple parameterization in August 2011. For this work, the used solar surface irradiance data are erroneous and are corrected in Nicolaus et al. [2013]. In order to improve that simple parameterization, the melt pond distribution and melt season duration is included as shown in Section 3.3. Furthermore, the ice type classification became more detailed concerning the seasonality to finally enable all-season estimates of the solar radiation under Arctic sea ice. Based on these new parameters the state of the Arctic sea ice in August 2011 and the consequential changed light distribution under sea ice is discussed in the following. A map with labeled regions of the Arctic Ocean is attached in the appendix material (Figure A.1). Indications of total heat fluxes stand for a spatial and temporal summing up of the given fluxes for the entire Arctic about a specified time.

In August 2011, the sea ice extent was $5.2 \times 10^6 \text{ km}^2$ with a mean sea ice concentration of 63 % (Figure 4.1a). Following the sea ice classification proposed by Maslanik et al. [2007], 56 % ($2.9 \times 10^6 \text{ km}^2$) was FYI, and the remaining 44 % ($2.3 \times 10^6 \text{ km}^2$) was MYI. MYI dominated the area along the Greenland coast to 60°E and along the Canadian coast in the Beaufort Sea to approximately 150°W (Figure 4.1b). FYI dominated between 150°W and 150°E up to 73°N and between 150°E and 60°W up to 80°N . The major part of the melting sea ice (see definitions of sea ice classes in Section 3.3.2) of both ice types was located between 130°W and 180°W south of 78°N . Hence, on average over August 2011 melting FYI covered 27 % of the entire FYI whereas only 14 % of the MYI melted anyway during that time.

The melt pond fraction on Arctic sea ice [Rösel & Kaleschke, 2012] was 31 % on the FYI and 33 % on the MYI surfaces on the monthly average (Figure 4.1c). Melt ponds were evenly distributed on FYI dominated areas, while the distribution on MYI dominated areas shows more spatial variability. The lowest fraction is located

4. Results

in the Greenland Arctic Basin between 0° and about 80°W on MYI with high ice concentration and melt pond fraction of about 25%. In contrast, the most melt ponds are detected between 100°W and 170°W in the area south of 85°N which is also dominated by MYI.

Furthermore, the solar surface radiation has a big influence on the light distribution under Arctic sea ice. It is shown that it was spatially and temporally averaged 110Wm^{-2} over the Arctic Ocean for August 2011 (Figure 4.1d). The minimum of 67Wm^{-2} was observed near Spitsbergen and above the European Arctic Basin while the maximum was found about the coastal regions, especially east of Greenland (up to 230Wm^{-2}). Summing up for August 2011, the total solar surface irradiance was $1.51 \times 10^7\text{Wm}^{-2}$ over the entire Arctic Ocean region north of 65°N .

Based on the previously described sea ice conditions and surface solar radiation as well as the developed transmittance of different ice types (Section 3.3.5), it was possible to estimate the transmitted light under Arctic sea ice. For that reason the transmitted solar radiation at the bottom of the ice is calculated for each single

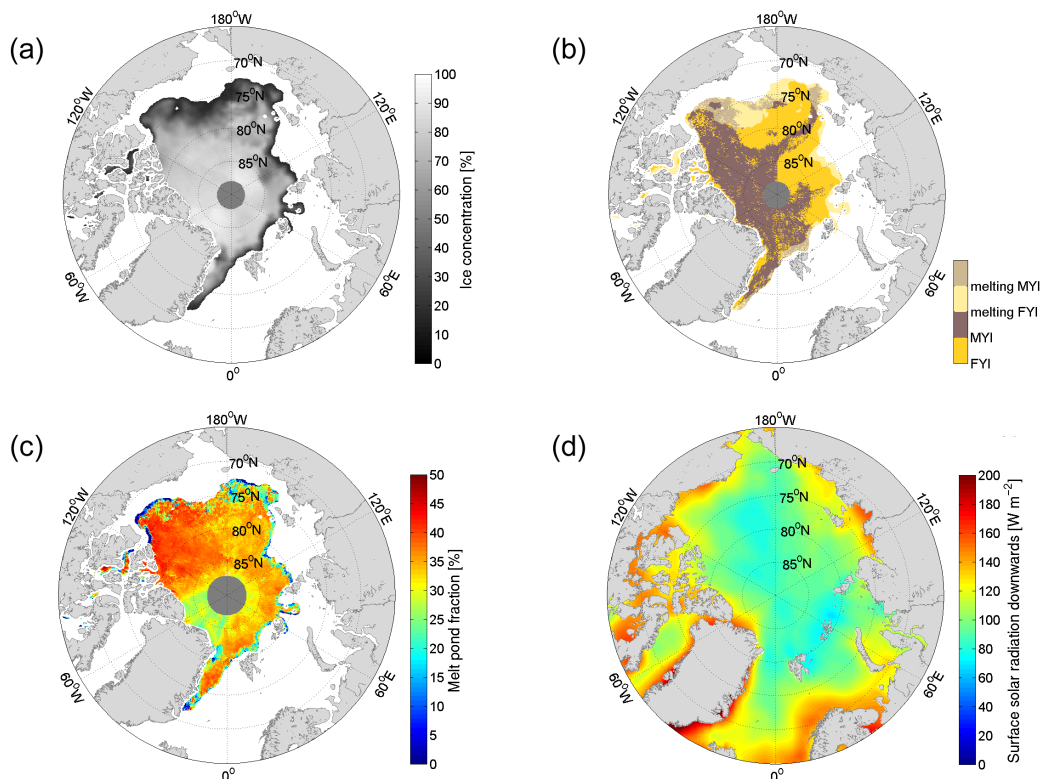


Figure 4.1.: Sea ice and atmospheric conditions in August 2011. (a) Sea ice concentration, (b) Ice type classification including melting classes, (c) Melt pond fraction, (d) Surface solar radiation downwards.

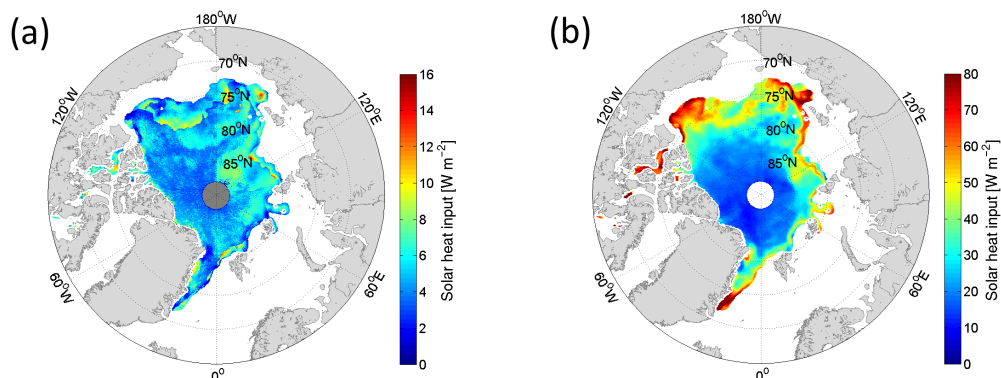


Figure 4.2.: (a) Solar heat input through Arctic sea ice in August 2011, excluding fluxes through open water. (b) Solar heat input into the Arctic Ocean through sea ice and open water in August 2011.

grid cell and each day according to Equation 2.10. The results of the solar heat input through Arctic sea ice to the upper ocean, excluding fluxes through open water, are shown in Figure 4.2a. The calculated absolute heat input into the ocean ranges up to 13.8 Wm^{-2} in August 2011. The figure shows a clear distinction between regions dominated by FYI and regions dominated by MYI with larger heat input through areas with predominant FYI. That implies a total solar heat input for the entire Arctic region of $2.68 \times 10^5 \text{ Wm}^{-2}$ in August 2011 which is composed of $1.76 \times 10^5 \text{ Wm}^{-2}$ through FYI and approximately half of that amount through MYI ($0.92 \times 10^5 \text{ Wm}^{-2}$). Furthermore, the spatial pattern of heat fluxes represents the difference between completely melting and lasting sea ice over the summer. It is shown that the highest heat fluxes through the ice occur in the marginal melting sea ice zone in the East Siberian Sea as well as on the transition areas of still high ice concentration. The mean heat flux through the sea ice was 5.13 Wm^{-2} of the entire Arctic in August 2011 resulting from the mean transmittance of the ice cover of 0.084.

Including the calculated fluxes through open water within the sea ice extent, the effect of sea ice concentration as well as the areas of melting sea ice become more obvious. Consequentially, fluxes within the sea ice extent reach up to 120 Wm^{-2} in the marginal ice zones in the East Siberian Sea, the Beaufort Sea as well as south of 75°N at the coast of Greenland (Figure 4.2b). Since the sea ice cover was dominated by permanent ice (i.e. not-melting ice), the mean solar heat input through the entire sea ice covered Arctic was 33.3 Wm^{-2} with a mean transmittance of 0.39. Thus, fluxes through ice and melt ponds contributed 14% of the entire available light under Arctic sea ice in August 2011.

4.2. Seasonality of solar radiation under Arctic sea ice

For the heat and energy fluxes under Arctic sea ice it is not enough to consider only one month (August) but rather an entire year concerning the annual budget and regional differences. Figure 4.3 gives an overview about the monthly mean solar irradiance under Arctic sea ice (ice covered areas only) from January to December 2011. Additionally, Table 4.1 summarizes the monthly mean and total solar radiation fluxes over and under the Arctic sea ice.

The total solar heat input from October to March is negligible with $0.14 \times 10^5 \text{ Wm}^{-2}$ for the entire Arctic. Therefore, these months are not discussed any further.

Associated with the decreasing sea ice concentration (see Figure B.1) and the snow melt onset in April, the solar heat flux under the sea ice increases in the Barents Sea and more weakly in the area of Fram Strait. These regions are in general described as the oceanic inflow regimes. Due to the rising sun and hence an increase of solar surface heat fluxes at the surface, also in the area of Bering Strait a weak increase of solar heat input under the ice is observed. Nevertheless, the transmittance of 0.005 through Arctic sea ice is negligible in April.

In May, the solar heat input increases especially in the Barents Sea related to the

Table 4.1.: *Monthly mean and total solar radiation fluxes over and under the Arctic sea ice cover in 2011: Transmittance of Arctic sea ice τ , total solar surface radiation $\sum E_d$ over the Arctic Ocean (65°N to 90°N), total solar radiation under the sea ice $\sum E_T$, mean solar radiation under the sea ice $\overline{OE_T}$. For month of $\sum E_d < 50 \times 10^5 \text{ Wm}^{-2}$ the solar radiation under the ice and transmittance are negligible (marked by '-').*

	τ	$\sum E_d [\text{Wm}^{-2}]$	$\sum E_T [\text{Wm}^{-2}]$	$\overline{OE_T} [\text{Wm}^{-2}]$
January	–	0.33×10^5	–	–
February	–	6.62×10^5	–	–
March	–	49.5×10^5	–	–
April	0.005	166×10^5	0.33×10^5	0.46
May	0.015	303×10^5	1.84×10^5	2.50
June	0.054	337×10^5	8.10×10^5	10.7
July	0.089	259×10^5	7.34×10^5	11.4
August	0.084	151×10^5	2.68×10^5	5.13
September	0.039	62.0×10^5	0.31×10^5	0.72
October	–	12.5×10^5	–	–
November	–	0.92×10^5	–	–
December	–	0.05×10^5	–	–

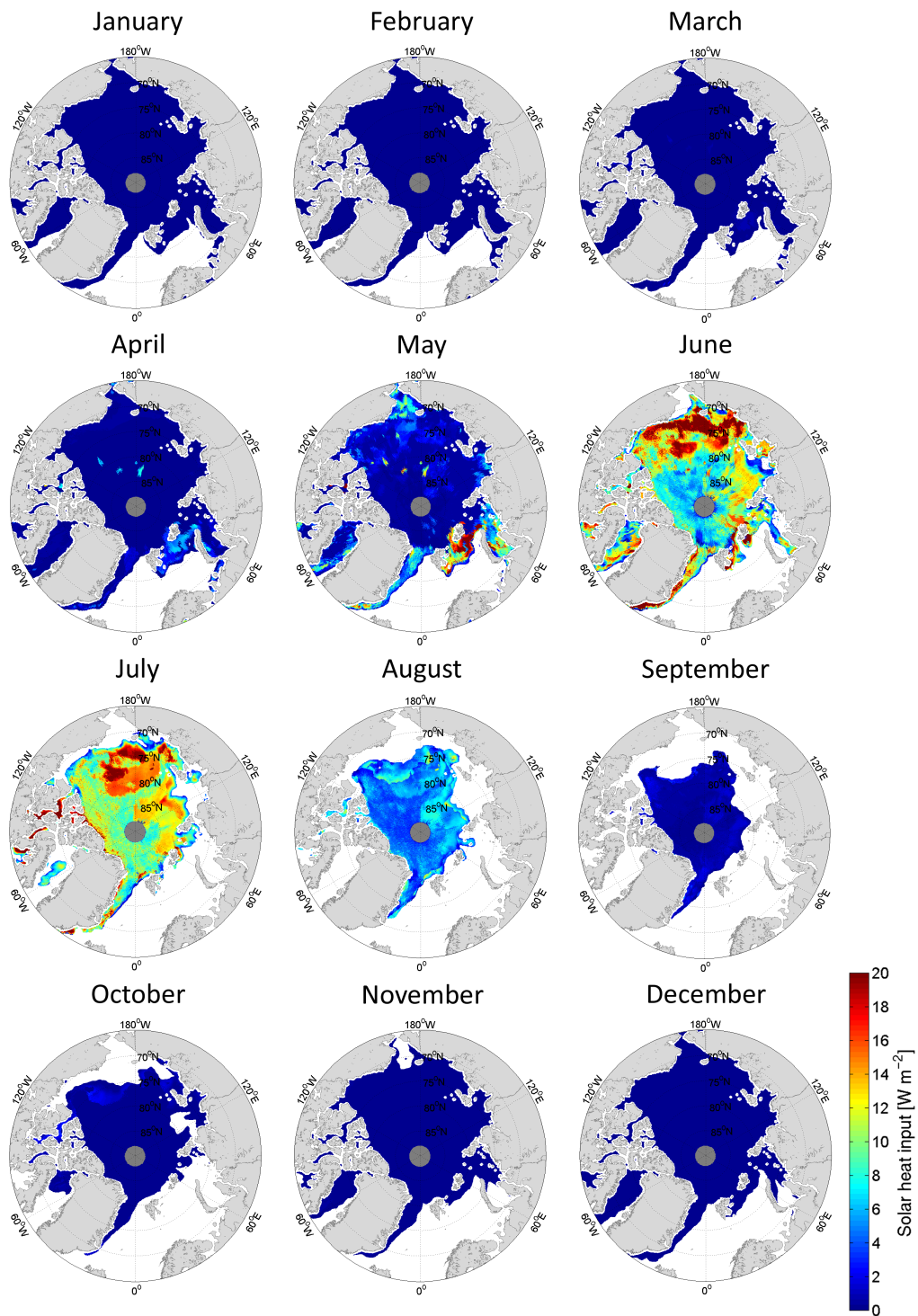


Figure 4.3.: Solar heat input through Arctic sea ice from January to December 2011, excluding fluxes through open water.

thinning of the ice cover which disappears during the month. The total solar heat input through the sea ice cover rises up to $1.84 \times 10^5 \text{ Wm}^{-2}$ in May implying a mean heat flux over the entire Arctic of about 2.50 Wm^{-2} . Associated with an almost doubling of the total solar surface irradiance ($303 \times 10^5 \text{ Wm}^{-2}$) over the entire Arctic Ocean, also the mean transmittance increases to 0.015.

In the transition period from May to June, the melt phase starts for large parts of the Arctic associated with a strong increase of light transmission through the ice cover. Also the total solar surface irradiance increases about 10% to $337 \times 10^5 \text{ Wm}^{-2}$. That high solar heat input connected with melting ice in these areas results in a distinctly increasing solar heat flux under the ice (up to 51 Wm^{-2}). Therefore, the light distribution under the sea ice cover is dominated by the shortwave solar heat input with weak influence of ice classification due to ice age but rather the distinction between completely melting ice and ice surviving the melting phase. All in all, June is the month of the highest total solar heat input through the ice ($8.10 \times 10^5 \text{ Wm}^{-2}$) associated with the highest solar irradiance over the Arctic Ocean.

During July, the sea ice extent decreases strongest. Due to the smaller ice covered region, the total solar heat flux through the ice decreases ($7.34 \times 10^5 \text{ Wm}^{-2}$) and more radiation penetrates directly into the ocean. Nevertheless, the mean solar heat input reaches its maximum of 11.37 Wm^{-2} resulting from a maximum mean transmittance of 0.089. The light distribution under sea ice is still mainly characterized by the solar irradiance with an increasing influence of the different ice classes. Hence, the distinction between thick MYI, much thinner FYI and melting ice areas is significant in the solar heat flux through the ice in July.

Due to an strong decrease in solar surface irradiance in August compared to the previous months, also the mean solar radiation under Arctic sea ice decreases by more than 50% to 5.13 Wm^{-2} (mean transmittance: 0.084). The decline in sea ice extent by 23% from July to August results mainly from reduction in FYI which decreased from $4.26 \times 10^6 \text{ km}^2$ to $2.88 \times 10^6 \text{ km}^2$.

In September the total solar heat input over the Arctic Ocean is $62 \times 10^5 \text{ Wm}^{-2}$ with an mean solar irradiance of 45 Wm^{-2} . The resulting mean radiation flux under the sea ice is 0.72 Wm^{-2} related to a low transmittance of sea ice of 0.039.

Summarizing, the total annual solar radiation under Arctic sea ice was $20.72 \times 10^5 \text{ Wm}^{-2}$ in 2011. Four months of the year (May to August) account for 96% ($19.95 \times 10^5 \text{ Wm}^{-2}$) of the total annual solar heat input through the sea ice. Including the months of April and September, 99% ($20.58 \times 10^5 \text{ Wm}^{-2}$) of the total annual flux under the sea ice cover are recorded. In contrast, 78% of the total solar surface irradiance are observed from May to August and 95% including again April and September.

Especially differences in available light over and under sea ice from May to August illustrate the importance of the surface properties, e.g. concerning the snow cover.

4.3. Development of light transmission from 1979 to 2011

To constitute the solar heat input through the sea ice cover into ocean during the entire period of satellite observations from 1979 to 2011, the total annual budgets related to regional differences as well as their trends are described in the following. The analysis concerning the significance of the trend of the time lines are performed by Mann-Kendall tests [Mann, 1945; Kendall, 1948]. The null hypothesis of the non-parametric trend assumes independent and randomly ordered data.

The mean solar heat input to the ocean within a grid cell for 1979 to 2011 underlies strong spatial variabilities and thus, ranges from about 50 to more than 2000 Wm^{-2} , as illustrated in Figure 4.4a. The maximum solar heat input occurs in the Canadian Arctic Archipelago and around Greenland. Another local maximum is observed in the East Siberian Sea and in parts of the Chukchi Sea (1200 Wm^{-2}). In comparison with the incident solar radiation (Figure C.1), these areas show also high fluxes. In addition, in the East Siberian Sea and Chukchi Sea the melting of sea ice on the surface starts earlier than in other regions. In contrast, the minimum solar heat input to the ocean occurs at the edge of the marginal ice zone in the Greenland Sea and Barents Sea. These regions are characterized by a strong spring sea ice retreat and thus, low sea ice concentration. The mean of the total annual under-ice flux in

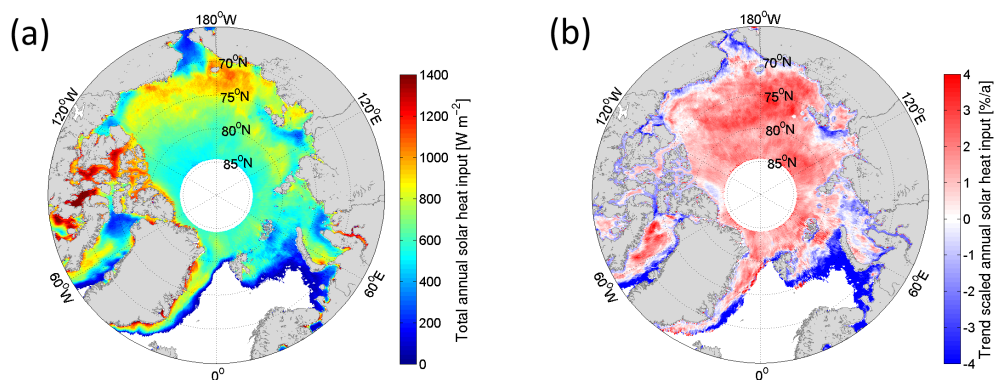


Figure 4.4.: (a) Mean total annual solar heat input through sea ice within a grid cell from 1979 to 2011. (b) Trend in total annual solar heat input through sea ice from 1979 to 2011. The trend is corrected for the trend in sea ice concentration.

the area of the mean sea ice extent is 660 Wm^{-2} .

Figure 4.4b illustrates the trend in the annual solar heat input through the ice cover to the ocean. The trend has been corrected for the trend in sea ice concentration. It is calculated by fitting the total annual heat flux of each grid cell with a polynomial function for the entire period from 1979 to 2011. The resulting trends are mostly positive but negative values occur in the seasonal marginal ice zone. These negative trends are associated with the reduction in sea ice concentration and extent. This is because the solar irradiance does not penetrate the ice anymore but rather goes directly into the ocean and is finally not considered as transmitting sea ice.

The positive trends of the total annual heat input through the ice within a grid cell range up to 10 \%a^{-1} with a mean of 1.6 \%a^{-1} . The strongest signal is observed in the East Siberian Sea and in the southern part of North American and Russian Arctic Basin.

Besides the solar surface irradiance, the sea ice concentration and the timing of the melting period, the transmittance influences the solar heat input through the ice to the ocean. Figure 4.5a illustrates an obvious increase for August from 1979 to 2011. Concerning the significance, it becomes apparent that the null hypothesis at the alpha significance level of less than 1% can be rejected for the time line. Hence, the transmittance has a distinct trend. The calculated increases is amounted to 0.9 \%a^{-1} . The strongest increase is shown during the last 6 years from 2005 to 2011. The transmittance increased from about 0.057 in 1979 to 0.067 in 2000, and to 0.084 in 2011. From 1979 to 2000 the mean transmittance is given as a constant proportion of melt pond and sea ice transmittance. Since 2000 information about the melt pond fraction is available, hence, the transmittance is calculated as a weighted mean of sea ice and melt pond fraction as given in Chapter 2.2. For comparison, Figure 4.5a shows also the mean transmittance without the input of the given melt pond fraction after 2000. Both curves show a good agreement in the trend.

Another parameter causing the minor increase in solar heat input to the ocean is the increasing melt season duration (Figure 4.5b). Here, especially the timing of the onset of melting conditions plays a crucial role. The time line suggests a trend towards earlier melt onset, shifting from day 145 (24 May) to day 141 (20 May), according to the linear regression. The timing of the mean EMO ranges for the entire period between day 137 and 147. At an alpha significance level of 3% the null hypothesis can be rejected for the EMO, so a trend in the data set is high significant.

4.3. Development of light transmission from 1979 to 2011

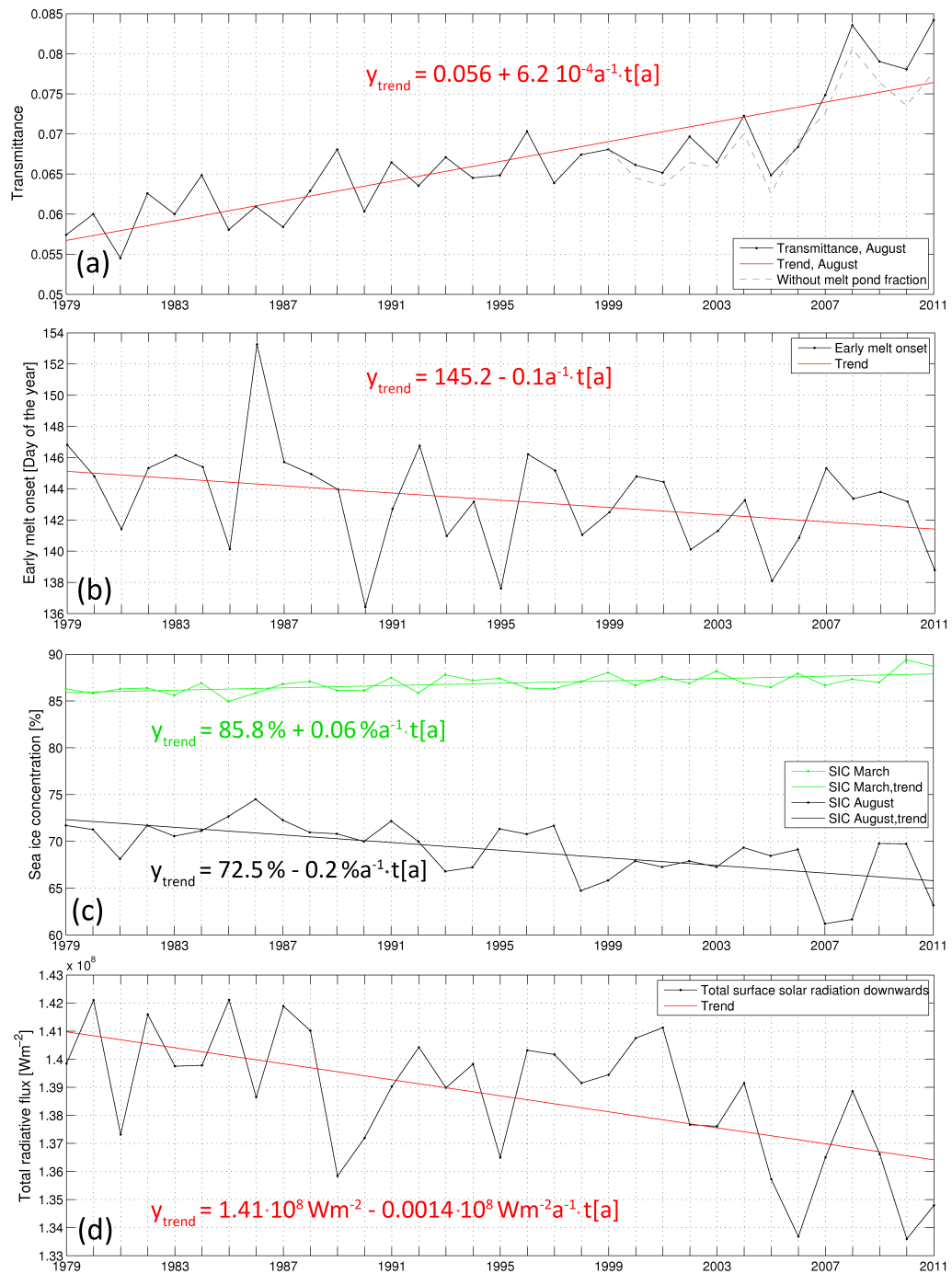


Figure 4.5.: (a) Mean transmittance (black) and its trend (red) as well as the calculated transmittance with a constant melt pond fraction (dotted gray line) for August 1979 to 2011. (b) Early melt onset (EMO) and its trend. (c) Sea ice concentration and its trend for August (black) and March (green). (d) Surface solar radiation and its trend. Additionally, the equations for the trends as a function of time t are given.

Also the decreasing sea ice concentration has a decisive influence on the trend of the solar heat input to the ocean. Although the month of sea ice maximum (March) shows of a weak increase in sea ice concentration, the general decrease is mainly caused in an increase of the summer retreat observed in August (Figure 4.5c). The strongest increase is observed in August but nevertheless, the sea ice concentration shows high variability around that month since 2007, connected to the pronounced sea ice minima. The Mann-Kendall test shows a trend for the sea ice concentration for both month at a confidence level of 99%.

The total annual solar irradiance on the surface of the Arctic Ocean shows also a weak negative trend of about $0.3\%a^{-1}$ (Figure 4.5d). Although the trend is significant (rejection of the null hypothesis at the 1% alpha significance level), the values are subject to strong annual variations.

Summarizing, all introduced parameters influencing the solar heat input through the Arctic sea ice show a significant behavior for their temporal evolution. Nevertheless, the transmittance has the most obvious and strongest trend and thus, the trend of the solar heat input through the sea ice to the ocean is crucially determined by the development of the transmittance.

4.4. Validation and sensitivity studies

4.4.1. Product validation using additional field data (Tara drift, 2007)

In order to validate the newly developed and described data product, it is useful to compare the calculated radiative fluxes under the sea ice cover with previously measured data. During the Arctic Transpolar Drift of Tara in 2007, continuous measurements of optical properties (albedo and transmittance) of snow and ice in the Arctic Ocean were performed from 29 April to 28 August 2007. Thus, an evaluation of the transition phase from spring to summer, summer itself, and the transition from autumn to winter is possible.

Since the actual daily position of Tara can not be mapped to a single grid point, the nearest-neighbor grid points of the Tara position were chosen. Both the heat fluxes through the sea ice as well as the transmittance were averaged for the put to six chosen grid points in order to compare these mean values with the Tara measurements. Figure 4.6 compiles measured and derived (a) incoming solar surface radiation, (b) total (broadband) transmittance and (c) transmitted solar radiation through the sea ice.

Considering the solar surface irradiance for the observation period the values range from about 350 Wm^{-2} in the beginning of June to less than 80 Wm^{-2} in the end of

August. Until the beginning of June, the measured radiation flux is smaller than the flux of the ECMWF data used for the calculations. Afterwards measured Tara data are higher than the ECMWF data. Causes for the mismatch between reanalysis and in-situ data might be uncertainties and simplifications of the ECMWF model, including local weather phenomena such as clouds, small pressure systems and anomalies.

Due to the an obvious connection between the time series of the transmittance and the transmitted light distribution under Arctic sea ice, both data sets are dis-

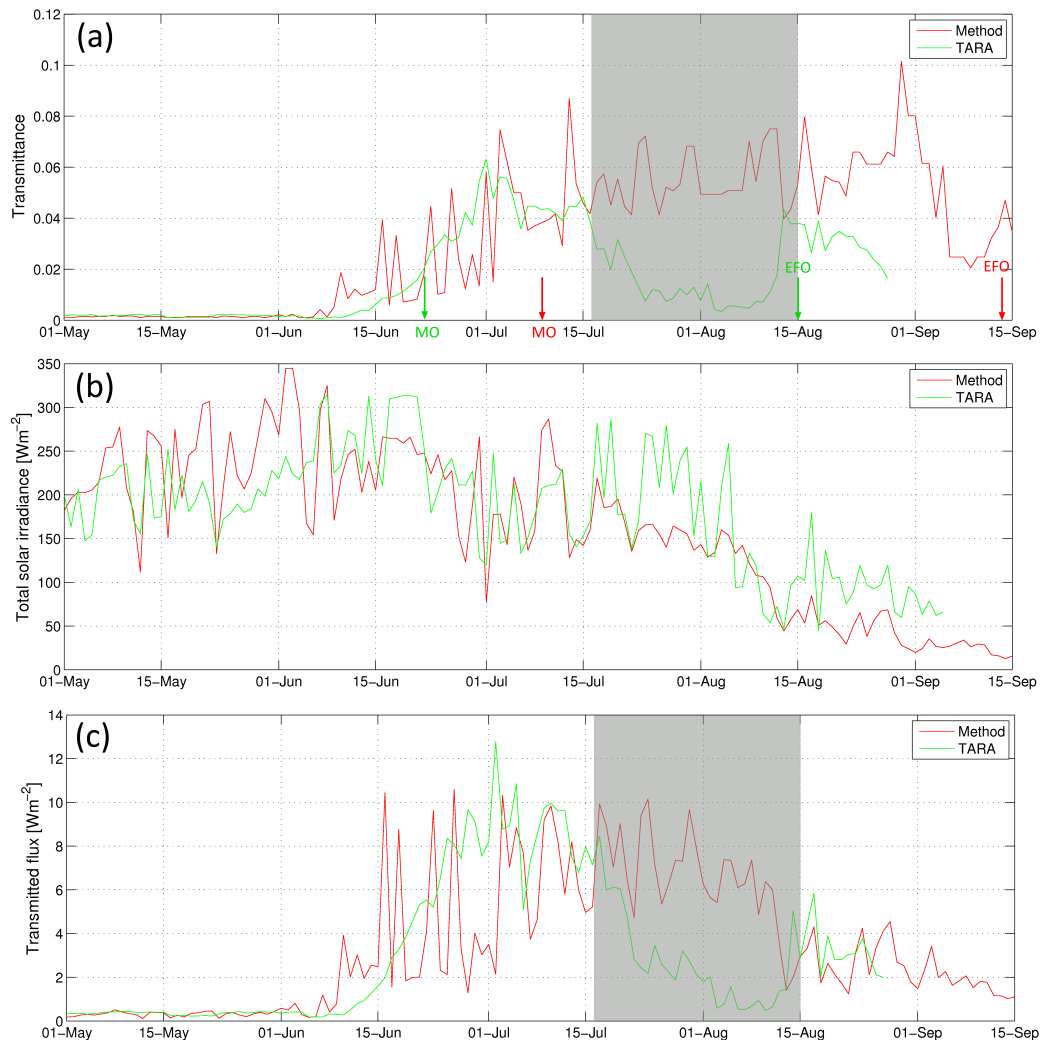


Figure 4.6.: (a) Transmittance, (b) total solar irradiance, (c) transmitted flux. Comparison between Tara measurements and MO/EFO (green) and calculated values and its MO/EFO using the developed method (red) in 2007. From 17 July to 14 August 2007 there is no useful comparison due to biological absorption (gray shaded).

cussed concurrently. Until 6 June, the measured and calculated transmittance vary weakly around 0.001, whereas the variations in the measured transmitted irradiance are much larger due to larger differences in the incoming solar radiation in both data sets. The early melt onset coincides between both data sets around 9 June. The subsequent increase in transmittance and transmitted irradiance during the transition time between spring and summer shows in general a similar behavior in both data sets. However, a closer view shows clear minima in the calculated transmittance (less than 0.015 instead of 0.03 to 0.06) as well as for the calculated transmitted light. Comparing these data points with adjacent grid cells, differences in the MO date are detected. The observed MO during the Tara drift was on 21 June; the MO of the surrounding data points was on 13 June and the MO of the minima was just the 8 July 2007. Hence, the high variability of the melt phase data set of Markus et al. [2009] over small areas accounts for these big differences in the transmittance and the transmitted fluxes. Late MO dates result in smaller calculated transmittance and consequently weaker radiation fluxes through the sea ice than measured during the field work at Tara.

Results during summer (14 July to 14 August) are difficult to compare. At Tara, biological activity increased absorption and leads to a significant decrease in transmittance. The measured solar radiation under the sea ice decreased to about 1 Wm^{-2} and also the transmittance is reduced to less than 0.01 at Tara. The calculated transmittance of this study varies around 0.07 during that period. However, the solar irradiance under the sea ice cover varies between 6 and 11.5 Wm^{-2} until the beginning of August, afterwards the heat flux decreased due to a lower sun elevation. With the end of the biological absorption in mid of August, the observed transmittance increased rapidly to about 0.043, comparable to the calculated transmittance. Subsequently, the observations point out the beginning of freezing conditions shown in the decreasing transmittance whereas the calculated transmittance remains on the summer level. Differences in the FO date are again the reason for the contrasting properties of both data sets. The observed EFO was on 15 August whereas the given data set maintains summer melt conditions almost one month longer, until 14 September. Hence, the transmittance stays at summer level and even increases in the end of August/ beginning of September. This is explained by a high melt pond fraction of more than 50 % in the chosen grid cells. Due to much lower solar surface irradiance in the reanalysis data than in the measured ones, the solar radiation under the Arctic sea ice was similar with fluxes between 1.5 and 4.8 Wm^{-2} . Concerning the total heat budget of both data sets from 1 May to 28 September 2007, the melting period from 17 July to 14 August 2007 has to be neglected due to the biological absorption. Thus, the total solar heat input through the sea ice

to the ocean was 248 Wm^{-2} for the measured Tara data from 1 May to 16 July 2007. For the same time and area the calculated data estimate a total heat flux of 203 Wm^{-2} . After the melt season (15 August to 28 August 2007), the total solar heat input through the ice is for both data sets approximately 42 Wm^{-2} .

4.4.2. Sensitivity study I: Changing length of melt season

Large discrepancies in the dating of melt onset are found to be the main reason for the mismatch between observed and calculated transmittance and transmitted light. Thus, a sensitivity study focusing on the influence of timing and length of the melt season on the solar heat input to the upper ocean is set up. Table 4.2 gives an overview about the implemented studies with the resulting transmittances and total solar heat fluxes under the Arctic sea ice cover. Since the developed method is based on measurements for the 2011, all following experiments are performed for this year.

For the study to lengthen the melting period, the day of early melt onset and melt onset is shifted backward (earlier in the year) or the day of early freeze up and the (continuous) freeze up is shifted forward (later in the year). 7 days earlier EMO and MO affect mainly the month of high ice concentration and high solar surface irradiance and result in an increase in total annual solar heat input through the ice to the ocean of 9 % from $20.7 \times 10^5 \text{ Wm}^{-2}$ to $22.6 \times 10^5 \text{ Wm}^{-2}$ for the entire year 2011. Thus, in April and May the strongest increases of about 21 to 22 % is obvious compared to the reference melt onset dates. The transmittance for August changed slightly from 0.084 to 0.085 due to few areas where EMO/MO occurred only in August or later that year.

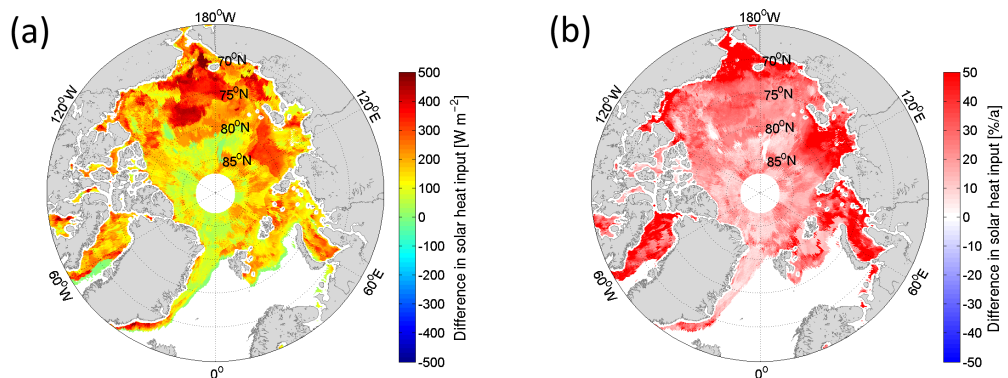


Figure 4.7.: Changes in solar heat input through the Arctic sea ice due to shifting the EMO/MO 14 days backwards compared to the default system. (a) Absolute variations [Wm^{-2}], (b) relative variations [%/a].

4. Results

Shifting the melt season in turn another 7 days (total 14 days) backward with the resulting mean EMO on 1 May and MO on 16 May, the increase of the solar heat flux under the ice more than double compared to the 7-day shift. Hence, the total annual heat input through the ice to the ocean increases by 20% to about $24.8 \times 10^5 \text{ Wm}^{-2}$ for the entire year. The pronounced increase is most evident in April with an increase of about 100% relating to the reference system, so a shift from $0.33 \times 10^5 \text{ Wm}^{-2}$ to $0.67 \times 10^5 \text{ Wm}^{-2}$ is calculated. The strongest absolute increase of $2.1 \times 10^5 \text{ Wm}^{-2}$ (transmittance from 0.054 to 0.067) is observed in June. Considering the impact of dating EMO/MO 14 days earlier compared to the default values, the largest variations of solar heat input to the upper ocean are found in the marginal sea ice zone, adding up to more than 100% (Figure 4.7b). However, strong correlation is observed between deviations and the supposed sea ice class (Figure 4.7a). Largest deviations of more than 500 Wm^{-2} are found in areas of melting sea ice, especially in the Chukchi Sea, whereas areas with dominating MYI are much less affected (up to 150 Wm^{-2}). Variations of solar heat fluxes under FYI range from 150 Wm^{-2} to 300 Wm^{-2} .

In comparison, the melt season may be extended by a 14 day later onset of freezing without changing EMO/MO. That amounts a 2% increase for the total flux from $20.7 \times 10^5 \text{ Wm}^{-2}$ to $21.0 \times 10^5 \text{ Wm}^{-2}$. Since the solar angle is too small to have any significant effect, the change in the end of the melt season affects just parts of August and September (increase of 35% with an increase from $0.31 \times 10^5 \text{ Wm}^{-2}$ to 0.42 Wm^{-2}).

Figure 4.8 shows Arctic-wide variations due to a 14 day later FO. Modifications in the central Arctic (excluding the Canadian Arctic Archipelago) range from -7 to

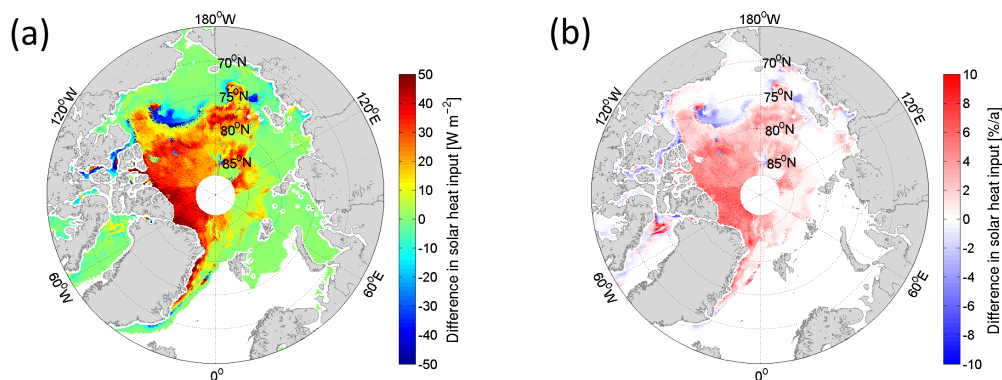


Figure 4.8.: Changes in solar heat input through the Arctic sea ice due to shifting the EFO/FO 14 days forwards compared to the default system. (a) Absolute variations [Wm^{-2}], (b) relative variations [$\%/a$].

7%, with positive variances in the area of the Greenland Arctic Basin, where high solar irradiance and sea ice concentration prevail. In regions of FYI transitioning to new MYI, the deviation is generally limited to 2% due to the predominantly low sea ice concentration.

If sea ice is formed after the EFO, it is masked as newly formed FYI and has a higher transmittance than FYI. A later EFO causes a longer existence of FYI and thus, a higher transmittance but a decreasing total annual solar heat flux through the sea ice in these regions. Thus, negative variances occur in areas of newly formed sea ice.

A 14 days later EMO/MO, and thus a shorter melt period, results in an increasing solar heat input through the ice to the ocean by 13% to $18.1 \times 10^5 \text{ Wm}^{-2}$ compared to the reference set up. April is again the month with the highest relative change detected by a decrease of about 24%. Due to the highest sun elevation, the strongest absolute decrease in solar irradiance under the sea ice cover occurs again in June where the total flux decreases from $8.10 \times 10^5 \text{ Wm}^{-2}$ to $6.66 \times 10^5 \text{ Wm}^{-2}$.

To summarize, it is shown that a change of the beginning of the melting period has a 14 times bigger impact than changes of the begin of the freeze up period concerning the generated change in the total transmitted heat fluxes. Reasons and consequences are discussed in Chapter 5.

4.4.3. Sensitivity study II: Changing transmittance and melt pond fraction

In the previous section, the influence of the melt season duration and timing on the light distribution under Arctic sea ice are shown. Another factor for the solar heat input through the ice to the ocean is the transmittance of the sea ice and the related melt pond fraction. The following sensitivity study quantifies the influence of both parameters on the resulting fluxes. To study the effect of transmittance, in the first experiment the transmittance of pure and ponded ice is changed by 10% relatively for the period from EMO to FO+60 days. For the second experiment, only the transmittance of bare ice is increased of 10%. The changes are implemented for the entire year except the winter period due to low light conditions. The resulting transmittances and total solar heat fluxes under the Arctic sea ice are compiled in Table 4.3. All experiments are performed again for 2011.

The result of the reduced pure and ponded ice transmittance is a decrease of the solar heat flux through the Arctic sea ice of 8% to a total flux of $19.1 \times 10^5 \text{ Wm}^{-2}$. As expected, the strongest reduction in solar heat input is in June ($-0.7 \times 10^5 \text{ Wm}^{-2}$) and the weakest one in April ($-0.01 \times 10^5 \text{ Wm}^{-2}$). An increase in transmittance

of 10 % affects the change in solar radiation under the sea ice in the same way. The total solar heat input to the upper ocean increases in that case by 9 % from $20.7 \times 10^5 \text{ Wm}^{-2}$ to $22.4 \times 10^5 \text{ Wm}^{-2}$. The maximum absolute changes in total solar irradiance are observed in June and July with deviations compared to the reference set up of 0.58 and $0.68 \times 10^5 \text{ Wm}^{-2}$, respectively.

Changing only the transmittance of the bare/white ice layer (excluding the melt ponds), the changes in solar radiation through the sea ice to the upper ocean are much weaker than for the both components of ice and melt ponds. Both, increasing and decreasing the sea ice transmittance of 10 % causes changes of about 2 % of the heat flux under the sea ice cover. Thus, an increase in transmittance implies a total solar heat input through the sea ice to the ocean of about $21.1 \times 10^5 \text{ Wm}^{-2}$, whereas a decrease leads to $20.4 \times 10^5 \text{ Wm}^{-2}$. The changes are broadly homogeneously distributed around the year with variations of 0 to 5 % per month in the solar radiation under the ice cover. The absolute changes range at this point from $0.01 \times 10^5 \text{ Wm}^{-2}$ in April to 0.15 Wm^{-2} in June.

Comparing the calculated variations due to changes in transmittance of bare and ponded ice and in transmittance of bare ice only, it is obvious that the bare ice transmittance has a crucially small impact. Hence, only 24 % of the increase in the solar radiation under Arctic sea ice are caused by the increasing transmittance of bare ice. The remaining variance is caused by the changing transmittance of ponded ice.

An increase of the melt pond fraction by 10 % (1.1 times the default melt pond fraction) leads to an increase of the total solar heat input to the upper ocean by about 5 % (i.e. up to approximately $21.8 \times 10^5 \text{ Wm}^{-2}$). The effect approximately scales linearly, hence increasing the melt pond fraction by 20 % results in an increased heat flux of $22.8 \times 10^5 \text{ Wm}^{-2}$, which equals an increase by 10 %. In contrast, decreasing the melt pond fraction by 20 %, the derived available solar radiation under ice declines also by 10 %. Both for increasing and decreasing melt pond fractions, June shows the largest variations due to the maximum in solar surface irradiance.

Table 4.2.: Monthly transmittances (τ) and total solar heat input ($\sum E_T$) through the sea ice for each month for the first sensitivity study concerning changes in the duration of the melt season.

		default	EMO/MO-7d	EMO/MO-14d	EFO/FO+14d	EMO/MO+14d
April	τ	0.005	0.006	0.009	0.005	0.001
	$\sum E_T$ [Wm^{-2}]	0.33×10^5	0.40×10^5	0.67×10^5	0.33×10^5	0.25×10^5
May	τ	0.015	0.021	0.025	0.015	0.011
	$\sum E_T$ [Wm^{-2}]	1.84×10^5	2.25×10^5	3.02×10^5	1.84×10^5	1.49×10^5
June	τ	0.054	0.060	0.067	0.054	0.045
	$\sum E_T$ [Wm^{-2}]	8.10×10^5	9.10×10^5	10.2×10^5	8.10×10^5	6.66×10^5
July	τ	0.089	0.092	0.093	0.089	0.081
	$\sum E_T$ [Wm^{-2}]	7.34×10^5	7.63×10^5	7.90×10^5	7.34×10^5	6.65×10^5
August	τ	0.084	0.085	0.086	0.091	0.081
	$\sum E_T$ [Wm^{-2}]	2.68×10^5	2.72×10^5	2.76×10^5	2.81×10^5	2.58×10^5
September	τ	0.039	0.039	0.039	0.054	0.039
	$\sum E_T$ [Wm^{-2}]	0.31×10^5	0.31×10^5	0.31×10^5	0.42×10^5	0.31×10^5
Jan - Dec	$\sum E_T$ [Wm^{-2}]	20.7×10^5	22.6×10^5	24.8×10^5	21.0×10^5	18.1×10^5
	Variation compared to $\sum E_T$ (default)		+9%	+20%	+2%	-13%

Table 4.3.: Monthly transmittances (τ) and total solar heat input ($\sum E_T$) through the sea ice for each month for the first part of the second sensitivity study concerning changes in the transmittance of ponded and bare ice or only bare ice.

		default	Changed transmittance of pure and ponded ice		Changed transmittance of bare ice	
			$\tau - 10\%$	$\tau + 10\%$	$\tau - 10\%$	$\tau + 10\%$
April	τ	0.005	0.004	0.005	0.004	0.005
	$\sum E_T [\text{Wm}^{-2}]$	0.33×10^5	0.32×10^5	0.34×10^5	0.32×10^5	0.34×10^5
May	τ	0.015	0.015	0.016	0.015	0.015
	$\sum E_T [\text{Wm}^{-2}]$	1.84×10^5	1.72×10^5	1.95×10^5	1.80×10^5	1.87×10^5
June	τ	0.054	0.048	0.058	0.053	0.055
	$\sum E_T [\text{Wm}^{-2}]$	8.10×10^5	7.40×10^5	8.78×10^5	7.94×10^5	8.24×10^5
July	τ	0.089	0.082	0.094	0.087	0.090
	$\sum E_T [\text{Wm}^{-2}]$	7.34×10^5	6.75×10^5	7.92×10^5	7.23×10^5	7.45×10^5
August	τ	0.084	0.078	0.090	0.082	0.087
	$\sum E_T [\text{Wm}^{-2}]$	2.68×10^5	2.48×10^5	2.88×10^5	2.63×10^5	2.74×10^5
September	τ	0.039	0.035	0.042	0.035	0.042
	$\sum E_T [\text{Wm}^{-2}]$	0.31×10^5	0.28×10^5	0.33×10^5	0.29×10^5	0.33×10^5
Jan - Dec	$\sum E_T [\text{Wm}^{-2}]$	20.7×10^5	19.1×10^5	22.4×10^5	20.4×10^5	21.1×10^5
	Variation compared to $\sum E_T$ (default)		-8%	+9%	-2%	+2%

Table 4.4.: Monthly transmittances (τ) and total solar heat input ($\sum E_T$) through the sea ice for each month for the second part of the second sensitivity study concerning changes of the melt pond fraction (MPF).

		default	MPF+10%	MPF+20%	MPF-10%	MPF-20%
April	τ	0.005	0.005	0.005	0.005	0.005
	$\sum E_T$ [Wm^{-2}]	0.33×10^5				
May	τ	0.015	0.015	0.016	0.015	0.014
	$\sum E_T$ [Wm^{-2}]	1.84×10^5	1.91×10^5	1.98×10^5	1.77×10^5	1.70×10^5
June	τ	0.054	0.057	0.060	0.050	0.047
	$\sum E_T$ [Wm^{-2}]	8.10×10^5	8.56×10^5	9.04×10^5	7.62×10^5	7.14×10^5
July	τ	0.089	0.092	0.098	0.083	0.080
	$\sum E_T$ [Wm^{-2}]	7.34×10^5	7.72×10^5	8.10×10^5	6.96×10^5	6.58×10^5
August	τ	0.084	0.087	0.091	0.080	0.077
	$\sum E_T$ [Wm^{-2}]	2.68×10^5	2.79×10^5	2.91×10^5	2.57×10^5	2.46×10^5
September	τ	0.039	0.040	0.040	0.039	0.038
	$\sum E_T$ [Wm^{-2}]	0.31×10^5	0.31×10^5	0.32×10^5	0.30×10^5	0.30×10^5
Jan - Dec	$\sum E_T$ [Wm^{-2}]	20.7×10^5	21.8×10^5	22.8×10^5	19.7×10^5	18.7×10^5
	Variation compared to $\sum E_T$ (default)		+5%	+10%	-5%	-10%

5 | Discussion and conclusions

The aim of the thesis is to develop a description of the seasonality of light transmittance through sea ice in order to provide estimates of the solar heat input to the upper Arctic ocean, spanning the entire year. For summer conditions, the analysis is based on ROV measurements from the ship-based TransArc field campaign in 2011. For the remainder of the year, other field campaigns as well as estimates based on physical considerations regarding optical properties of ice and snow provide the basis for the analysis. Combining the derived parameterizations for the transmittance with reanalysis and satellite data, Arctic-wide estimates of available light under sea ice have been obtained. The approach to modeling the optical properties of the Arctic sea ice cover for the whole year includes an ice type classification (distinguishing FYI and MYI) and additional data on the onset of melting and freezing season, respectively. This approach is necessary as to accommodate the lack of time series of large-scale sea ice thickness and snow depth data sets. Furthermore, studies on seasonality of the under ice solar irradiance as well as time series analysis to discover trends have been carried out. In the following, seasonality, trend and future development of light transmission, as well as limits of applicability and related uncertainties are presented.

5.1. Seasonality of light transmission

Assessing solar heat fluxes under Arctic sea ice for 2011, the annual cycle decomposes into three phases: (1) winter (October to March), (2) mainly solar surface radiation-affected months (April to June) and (3) mainly ice-type-affected months (July to September). Since 99% of the total annual solar heat input through the sea ice is observed from April to September, winter can be neglected for the consideration of the seasonal light distribution under sea ice.

From April to May, the solar heat flux under sea ice is mainly affected by the oceanic inflow regimes of the Barents Sea and Fram Strait. Due to the imported oceanic heat flow, the ice is thinning in that region from below. The subsequent melting of the ice and snow in the marginal sea ice zone during the first weeks of available sun

light results in relatively high heat fluxes of up to 34.6 Wm^{-2} through the sea ice cover. During this time, the optically thick snow is converted to melting snow and the distinction between FYI and MYI becomes clearly apparent, as well as differences between melting and persistent ice. Although melting sea ice contributes less than 40 % to the total sea ice in June, it accounts for more than 55 % of the under ice heat flux for that month. As solar elevation angle decreases in July, differences between thick MYI and thinner FYI become more pronounced.

Hence, it is found that in August 2011 only one third of the total monthly solar heat input to the upper ocean is transmitted through MYI ($0.92 \times 10^5 \text{ Wm}^{-2}$) and about two thirds through FYI ($1.76 \times 10^5 \text{ Wm}^{-2}$). Considering in addition the development of the sea ice age during the last decades (Chapter 1.2, Maslanik et al. [2007]), a decrease in MYI coverage as well as a total disappearance of ice older than 4 years is clearly indicated. Consequently, the shift towards more FYI implies a higher solar heat input through the sea ice cover for the next years [Nicolaus et al., 2012].

In general, it is shown that the seasonal regional distribution of light under Arctic sea ice is strongly affected by the regional distribution of solar surface irradiance which is influenced by the cloud cover, by the dominant sea ice type and especially by the snow cover on top. Based on these results, May to August can be considered as the most important months regarding the transmittance of Arctic sea ice and the energy budget, as 96 % of the total annual solar heat input occurs during this time.

Compared to the monthly mean solar heat fluxes through the sea ice to the ocean calculated from SHEBA data presented in Huwald et al. [2005], the fluxes calculated in this thesis are half of that for the transition time (April/May). For the following time, the variation of about 10 % is in a similar range with the SHEBA data. The differences during April and May might be caused by the assumed constant transmittance of ice and snow of 0.08. The transmittance might be much lower due to a still big amount of optically thick snow for this time frame.

Hudson et al. [2013] present measured heat fluxes and calculated transmittances and albedo of Arctic FYI in the time range of the end of July to beginning of August 2012. Although the derived albedo of ponded (0.21) and white ice (0.55) fit reasonable good with those calculated in Nicolaus et al. [2012] (ponded: 0.21, white: 0.51), the resulting transmittances differ significantly (Nicolaus et al. [2012]: 0.22, 0.04; Hudson et al. [2013]: 0.32, 0.11). Also the calculated mean transmittance of FYI of 0.087 in this thesis is approximately 50 % lower than the one found by Hudson et al. [2013] of 0.16. These lower values occur despite assuming a lower melt pond fraction (23 % vs. 26 % in this thesis). The differences are on the one

hand caused by a thinner sea ice cover in July/August 2012 [Hudson et al., 2013] than in August 2011 [Nicolaus et al., 2012] (mean ice thicknesses of 0.8 m compared to 1.26 m). On the other hand, the different way of deriving the transmittances in both cases leads to the large differences. Nicolaus et al. [2012] use modal values derived from the histogram (see Figure 3.1) representing kind of level ice (white and ponded ice) conditions, whereas Hudson et al. [2013] calculate an average albedo and transmittance for each surface type.

5.2. Weaknesses and possible improvements of the presented method

The transition periods from spring to summer and summer to autumn are the critical phases of the year for the calculation of solar heat fluxes under Arctic sea ice. On the one hand, this is caused by the existing and changing layer of snow, which affects the light distribution under different types of sea ice crucially. On the other hand, validation studies based on the Tara field campaign in 2007 show large differences and uncertainties between the measured field data and the calculated data with the method concerning the timing of the melt season. These differences in the EMO and EFO lead to variances in the results of up to 70 % in the solar heat flux through the sea ice cover during this transition time. Thus, the timing and duration of the melt season have a crucial impact on the light distribution under Arctic sea ice. Due to the low solar surface irradiance during winter time, the uncertainties and errors for the calculations are much lower than during summer.

To study the effect of the timing of the melt season, sensitivity studies have been performed. Therefore, EMO and EFO were shifted backward and forward. It is shown that an EMO/MO timed 14 days earlier in the year has a much bigger impact on the solar heat input through the ice to the ocean (increase by 20 % for total annual heat flux) than an EFO/FO timed 14 days later (increase by 2 %). The changes in solar heat input due to the shifting EMO/MO are significant mostly for the monthly budget from April to June related to an increasing solar elevation angle and a thinning sea ice cover during this time. Also the comparison with the Tara data set shows especially for the period between EMO and the begin of summer melting large differences. Thus, the total heat flux through the sea ice calculated with the presented method obtains only 81 % of the total measured flux under sea ice during Tara from 1 May to 15 July. These differences are mainly caused by the high variability of the melt onset data set and the consequently shift of about 2 weeks between the observed melt onset during Tara and the used one for the cal-

culuation. Besides, uncertainties regarding the selection of the transmittances must be taken into account. For the transmittance of pure and ponded ice respectively one mode (in all cases the strongest mode) is selected to present the particular ice type.

Furthermore, Rösel & Kaleschke [2012] emphasize that the previous validations for the melt pond data set are not sufficient. The presented sensitivity study concerning a changing melt pond fraction ($\pm 20\%$) show changes in the total solar heat input through the ice to the ocean in the range of $\pm 10\%$. In addition, Rösel & Kaleschke [2012] point out an increase in the relative melt pond fraction of about 2.4% between 2000 and 2011. That increase leads also to an extension of the melt season due to its increased energy input.

Furthermore, it must be considered that all data sets used here include uncertainties and errors which are accumulated in the presented method. Thereby, the overall highest uncertainties stem from dating the melting and freezing phase as shown before. Due to this fact, the given variations by the shift of the melt onset are assumed as the uncertainties of the presented method. Figure 5.1 shows the total annual solar heat input to the ocean in 2011, as well as the associated uncertainty estimate.

Considering the shown weaknesses, it must be considered whether it is reasonable to use the data set of melt and freeze onset dates or whether the usage of additional data sets could improve the current method. Those additional data sets could include on the one hand satellite data products concerning the ice thickness or surface temperature to involve further information about changing surface properties. On the other hand, enhanced knowledge about snow thickness and properties could be obtained by additional large-scale observations focused on an all-season coverage of data reached e.g. by buoys and drift stations (as SHEBA or TARA). Also ROV

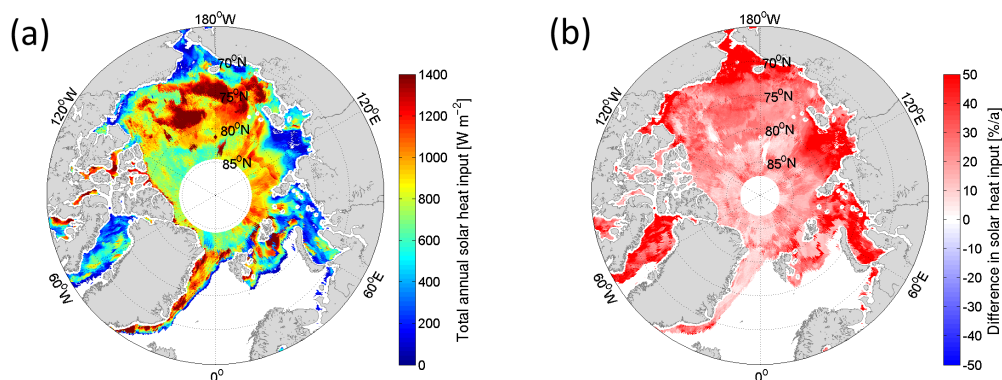


Figure 5.1.: (a) Total annual solar heat input through the sea ice to the ocean [Wm^{-2}] and (b) its error estimate [$\%/a$].

measurements as presented in Nicolaus et al. [2012] performed earlier in the year could help to improve and validate the new method concerning the optical properties of sea ice and snow. By combining all these data sets a more precise detection of the begin and the end of the melt season is expected. Further airborne observations and measurements could also improve and validate the detection of melt ponds on Arctic sea ice.

5.3. Trends of light transmission from 1979 to 2011 and future implications

The development of the solar heat flux through the Arctic sea ice during the past decades indicates an obvious increase. However, these changes are not homogeneously distributed but rather vary spatially. The strongest increase is shown in the Chukchi Sea as well as in the area of the East Siberian Sea. Reason might be no appreciable changes in sea ice surface properties but an obvious extended melt season. These developments imply an increase in transmittance (August 1979: 0.057, August 2011: 0.084) of the ice. Assuming an identical sea ice extent in 1979 as in 2011, the increase in the annual mean solar heat flux through sea ice amount to 53 % from 1979 to 2011.

Considering the presented results, it should be noted that the input data sets for the sea ice concentration and the melt and freeze onset consist of different data products because of changes in measuring and processing methods. Nevertheless, these changes are not noticeable in the consideration of the mean values for the entire Arctic. The results have therefore not been corrected with respect to discontinuities or similar artifacts.

Comparing the results with the development the solar heat input into the ice in Perovich et al. [2011], a weaker trend in the contribution of solar heat to the ocean compared to the solar heat input through the ice is evident. That different behavior is an indication of an increasing bottom and internal melt during the last decades and thus, affecting the sea ice mass balance. The increasing absorption of Arctic sea ice through a trend towards more seasonal and less multi year ice is also given in Nicolaus et al. [2012].

Maslanik et al. [2007] finds an obvious change in sea ice age during the past decades. It is shown that the amount of MYI decreases rapidly with an almost complete disappearance of ice older than 4 years. Hence, in 2011 only one third of the solar heat input through the sea ice is transmitted through MYI.

While the snow on MYI is accumulating through the entire fall and winter, at the

same time, the FYI is only forming, so less snow accumulates on newly formed sea ice. Related to a thinner snow cover on FYI, the formation of melt ponds during the spring and summer melt occurs much earlier in the season than on MYI. The increasing melt pond fraction on Arctic sea ice between 2000 and 2011 has been shown in Rösler & Kaleschke [2012]. A thinning of sea ice and more and deeper melt ponds on the sea ice surface lead to a deeper light penetration to the underlying ocean layer. Frey et al. [2011] show that light transmission through melt ponds have their maximum at the underside of the ice, followed by a monotonically decrease with depth. In contrast, the depth profiles under bare ice show the influence of relatively large light transmission through the adjacent melt ponds. That results in an increase of transmitted heat flux with depth up to a maximum of 5 to 10 m (depending on geometry), followed by an exponential increase with depth. Consequently, a higher melt pond fraction influences not only the light transmission through the melt ponds but rather the vertical light field under the adjacent bare ice fields. Beside important implications of the available light for the primary production and biogeochemical processes beneath the sea ice, also the temperature of the upper ocean mixed layer is increasing. Consequently, physical processes like bottom and internal melting become more important which result in an additional increase in transmittance of the sea ice. These feedback processes can be summarized as a 'transmittance-melt feedback': An increase of light transmission through sea ice imply an increasing internal and bottom melting which leads to a further increasing transmittance. The extended melt season leads furthermore to the possibility of forming of more leads and polynyas. These sea ice features allow the direct interaction between the atmosphere and ocean and thus, act as an important heat exchange and deposit area for the region. Hence, the lateral melting is increasing as well. In addition, higher melt pond fractions and thinner (so consequently darker) ice imply an increasing light absorption of sea ice resulting in a decreasing reflection.

Sensitivity studies indicate that especially the timing and length of the melt season have the most important impact on the annual solar heat flux under Arctic sea ice. Between 2007 and 2011 the begin of the melt season shifted almost one week forward implying an increased mean transmittance from 0.075 in August 2007 to 0.084 in August 2011. Assuming for the future the same positive trend in the EMO, the solar heat flux through the ice to the ocean will presumably increase until 2015 by about 9% due to a lengthened melt season. The increasing amount of heat under the sea ice cover implies also an increasing bottom melt and thus, an increasing transmittance and decreasing reflection of the sea ice. Altogether, this implies an amplification of the ice-albedo and transmittance-melt feedback. Furthermore, a thinner sea ice cover means also a stronger heat transport from the sea ice bottom

to the atmosphere during the freezing phase. Hence, the sea ice grows faster and is able to get thicker again, so the transmittance is decreasing and the albedo is increasing again. At which point that reversal to a decreasing transmittance and increasing albedo will occur, can not be answered in this thesis. It can be assumed that the impact of transmitted heat fluxes through the ice will become more and more important. This affects not only the mass and energy balance of sea ice, oceanic currents and stratification, but also biological processes in and under the sea ice.

All data sets used for this analysis are going to continue for the next years. Furthermore, model data could be used as input values for the calculations as well as an additional validation data set. Additionally, the developed parameterization of the transmitted fluxes could be involved in already existing models.

A | Regions of the Arctic Ocean

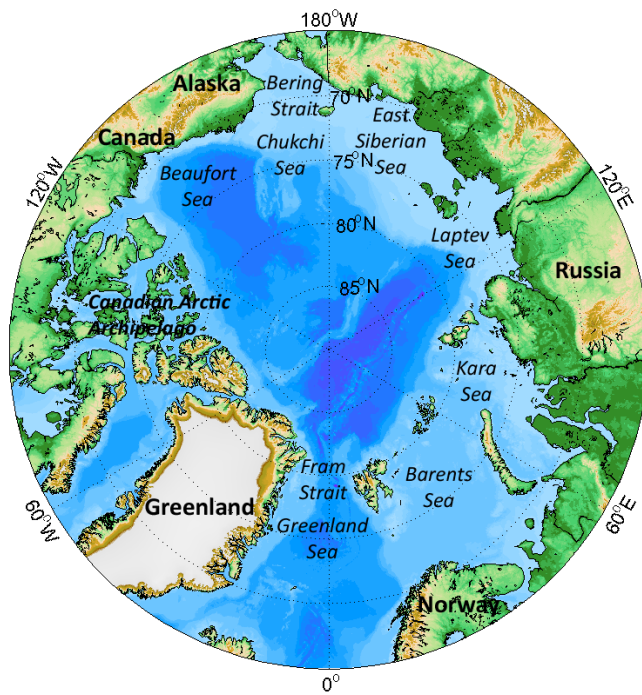


Figure A.1.: *The Arctic Ocean and its labeled main seas. Figure is based on Serreze & Barry [2005].*

B | Seasonality of sea ice concentration and surface solar radiation in 2011

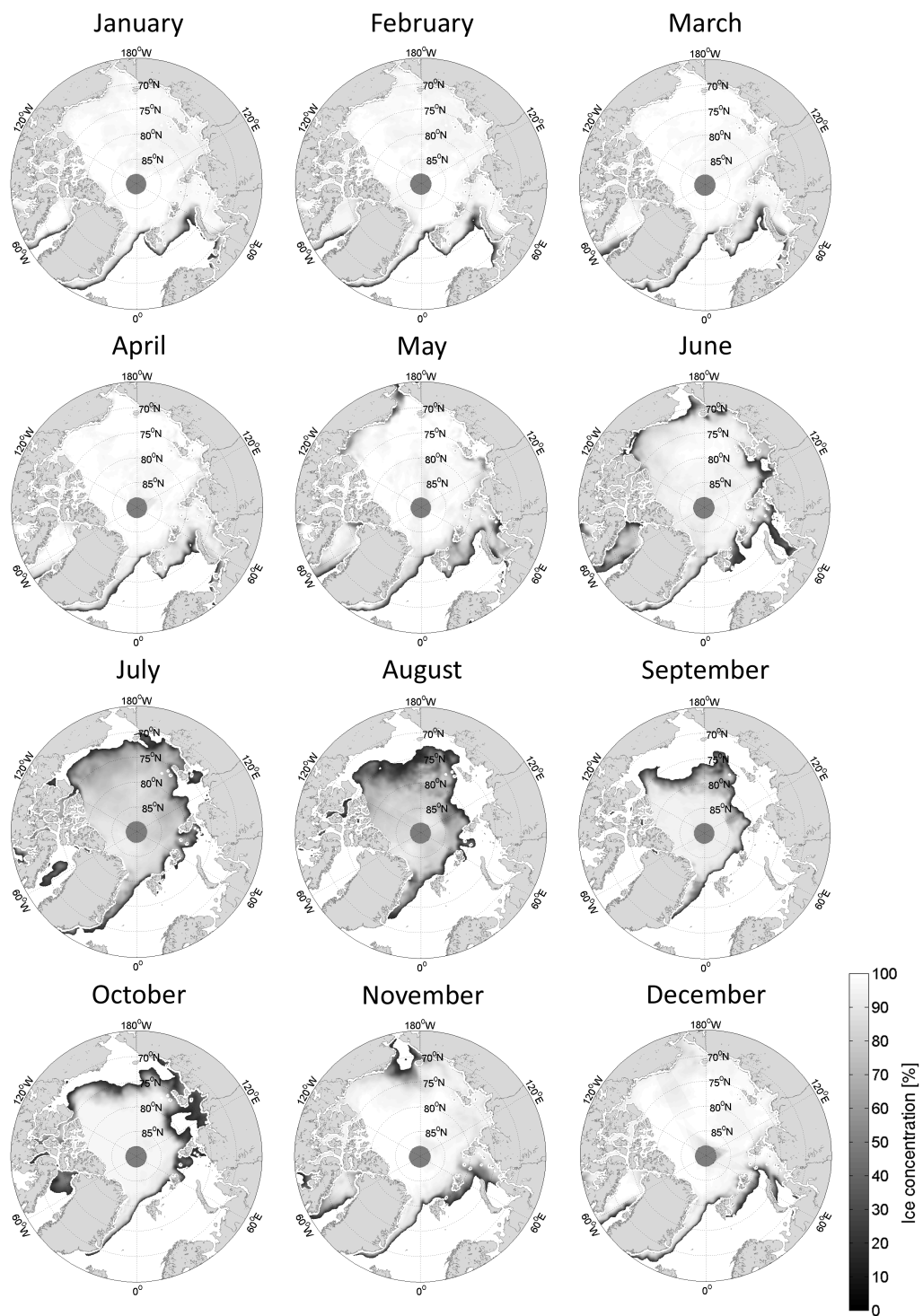


Figure B.1.: Sea ice concentration from January to December 2011 (sea ice concentration bigger than 15 %).

B. Seasonality of sea ice concentration and surface solar radiation in 2011

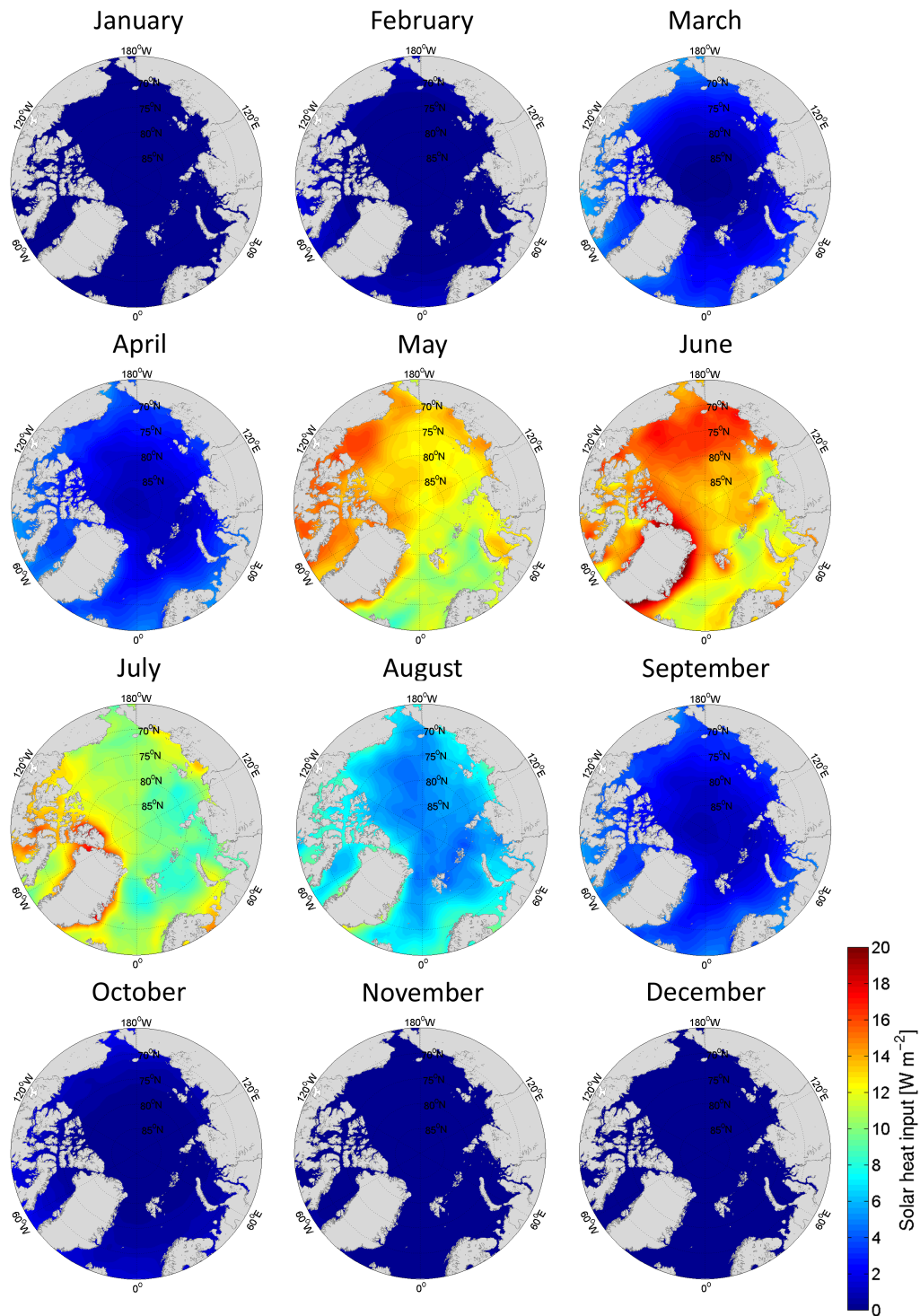


Figure B.2.: Solar surface radiation from January to December 2011.

C | Mean total surface solar irradiance from 1979 to 2011

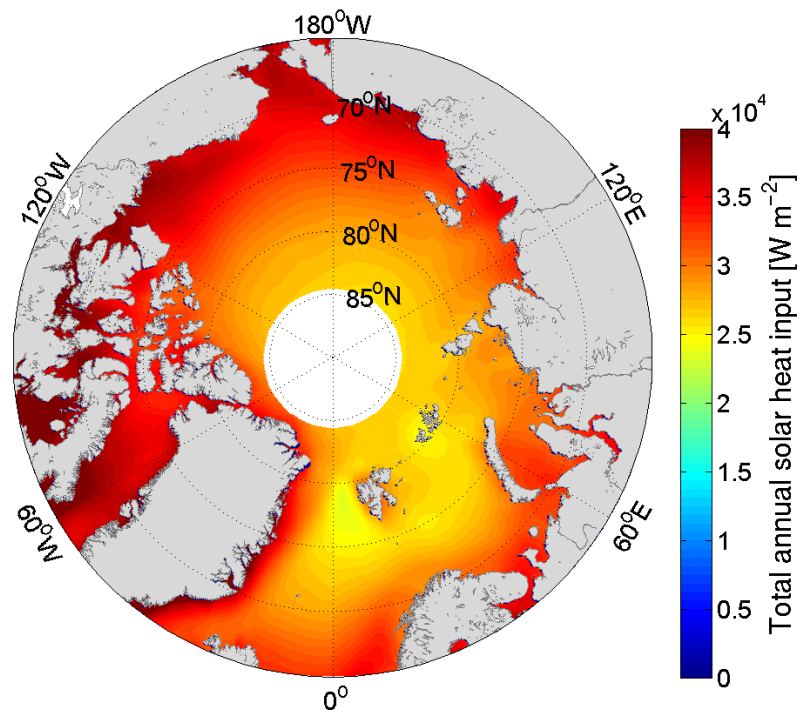


Figure C.1.: Mean total annual solar surface irradiance from 1979 to 2011.

List of Figures

1.1. Anomalies of Arctic sea ice extent in March and September.	3
1.2. Sea ice age from 1983 to 2011.	4
2.1. Range of observed values of total albedo for sea ice.	9
2.2. Influence of surface conditions on light transmittance through Arctic sea ice.	10
2.3. Schematic of the surface heat budget of Arctic sea ice.	13
3.1. Histogram of transmittances measured during TransArc 2011.	19
3.2. Solar heat input into the Arctic Ocean through sea ice, August 2011 [Nicolaus et al., 2012]	20
3.3. Mean melt pond fraction in August 2011.	22
3.4. Characteristic melting and freezing days as day of the year in 2011 .	24
3.5. Annual cycle and development of the surface properties and ice clas- sification of Arctic sea ice.	26
3.6. Progress of the transmittance of Arctic sea ice for the entire system of ice, snow and melt ponds.	29
3.7. Progress of the transmittance of Arctic sea ice for bare ice.	34
4.1. Sea ice and atmospheric conditions in August 2011.	38
4.2. Solar heat input into the Arctic Ocean through sea ice and open water in August 2011.	39
4.3. Solar heat input into the Arctic Ocean through sea ice for the entire year 2011.	41
4.4. Total solar heat input through sea ice and its trend for 1979 to 2011.	43
4.5. Timelines and trends for the parameter transmittance, EMO, sea ice concentration and surface solar radiation from 1979 to 2011.	45
4.6. Comparison of transmittance, total irradiance and transmitted flux between Tara measurements and calculated values in 2007.	47

4.7. Changes in solar heat input through sea ice due to shifting EMO/MO in 2011.	49
4.8. Changes in solar heat input through sea ice due to shifting EFO/FO in 2011.	50
5.1. Total annual solar heat input through the sea ice and its estimated error.	60
A.1. The Arctic Ocean and its labeled areas.	I
B.1. Sea ice concentration for the entire year 2011.	III
B.2. Solar surface radiation for the entire year 2011.	IV
C.1. Total solar surface irradiance from 1979 to 2011.	V

List of Tables

2.1. Monthly and annual means of the energy budget components from SHEBA 1997/98.	14
3.1. Data description	18
3.2. Measured and calculated transmittances during summer of different ice classes.	21
3.3. Declared and discussed transmittances for the entire year subdivided in different phases and ice types.	30
4.1. Monthly mean and total solar radiation fluxes over and under the Arctic sea ice cover in 2011.	40
4.2. Results of the first sensitivity study concerning changes in the duration of the melt season.	53
4.3. Results of the first part of the second sensitivity study concerning changes in the transmittance.	54
4.4. Results of the second part of the second sensitivity study concerning changes of the melt pond fraction.	55

Bibliography

- [Boetius et al. 2013] BOETIUS, Antje ; ALBRECHT, Sebastian ; BAKKER, Karel ; BIENHOLD, Christina ; FELDEN, Janine ; FERNÁNDEZ-MÁNDENZ, Mar ; HENDRICKS, Stefan ; KATLEIN, Christian ; LALANDE, Catherine ; KRUMPEN, Thomas: Export of Algal Biomass from the Melting Arctic Sea Ice. In: *Science* (2013).
- [Briegleb & Light 2007] BRIEGLEB, BP ; LIGHT, B: A Delta-Eddington multiple scattering parameterization for solar radiation in the sea ice component of the Community Climate System Model. NCAR Tech / Note NCAR/TN-472+ STR, National Center for Atmospheric Research. 2007. – Forschungsbericht.
- [Dee et al. 2011] DEE, D.P. ; UPPALA, S.M. ; SIMMONS, A.J. ; BERRISFORD, P. ; POLI, P. ; KOBAYASHI, S. ; ANDRAE, U. ; BALMASEDA, M.A. ; BALSAMO, G. ; BAUER, P. et al.: The ERA-Interim reanalysis: Configuration and performance of the data assimilation system. In: *Quarterly Journal of the Royal Meteorological Society* 137 (2011), Nr. 656, S. 553–597.
- [Eastwood 2012] EASTWOOD, S.: OSI SAF Sea Ice Product Manual. In: *OSI SAF Documentation* (2012), Nr. 3.8.
- [Francis & Vavrus 2012] FRANCIS, Jennifer A. ; VAVRUS, Stephen J.: Evidence linking Arctic amplification to extreme weather in mid-latitudes. In: *Geophysical Research Letters* 39 (2012), Nr. 6.
- [Frey et al. 2011] FREY, Karen E. ; PEROVICH, Donald K. ; LIGHT, Bonnie: The spatial distribution of solar radiation under a melting Arctic sea ice cover. In: *Geophysical Research Letters* 38 (2011), Nr. 22.
- [Gosselin et al. 1986] GOSSELIN, Michel ; LEGENDRE, Louis ; THERRIAULT, Jean-Claude ; DEMERS, Serge ; ROCHET, Martine: Physical control of the horizontal patchiness of sea-ice microalgae. In: *Mar Ecol Prog Ser* 29 (1986), Nr. 3, S. 289–298.

- [Grenfell & Perovich 1984] GRENFELL, T. C. ; PEROVICH, D. K.: Spectral albedos of sea ice and incident solar irradiance in the southern Beaufort Sea. In: *Journal of Geophysical Research-Oceans* 89 (1984), Nr. NC3, S. 3573–3580. – Times Cited: 139 Grenfell, tc perovich, dk.
- [Hakkinen et al. 2008] HAKKINEN, S. ; PROSHUTINSKY, A. ; ASHIK, I.: Sea ice drift in the Arctic since the 1950s. In: *Geophysical Research Letters* 35 (2008), Nr. 19. – Times Cited: 16 Hakkinen, Sirpa Proshutinsky, Andrey Ashik, Igor.
- [Harder et al. 1998] HARDER, Markus ; LEMKE, Peter ; HILMER, Michael: Simulation of sea ice transport through Fram Strait: Natural variability and sensitivity to forcing. In: *Journal of geophysical research* 103 (1998), Nr. C3, S. 5595–5606.
- [Hudson et al. 2013] HUDSON, Stephen R. ; GRANSKOG, Mats A. ; SUNDFJORD, Arild ; RANDELHOFF, Achim ; RENNER, Angelika H. ; DIVINE, Dmitry V.: Energy budget of first-year Arctic sea ice in advanced stages of melt. In: *Geophysical Research Letters* (2013).
- [Huwald et al. 2005] HUWALD, H. ; TREMBLAY, L.B. ; BLATTER, H.: Reconciling different observational data sets from Surface Heat Budget of the Arctic Ocean (SHEBA) for model validation purposes. In: *Journal of Geophysical Research* 110 (2005), Nr. C5.
- [Katlein 2012] KATLEIN, C.: *ROV basierte Untersuchung der räumlichen Variabilität der Lichttransmission durch arktisches Meereis im Sommer*, Eberhard Karls Universität Tübingen/ Alfred-Wegener-Institut für Polar- und Meeresforschung, Diploma thesis, 2012.
- [Kay et al. 2008] KAY, J. E. ; L’ECUYER, T. ; GETTELMAN, A. ; STEPHENS, G. ; O’DELL, C.: The contribution of cloud and radiation anomalies to the 2007 Arctic sea ice extent minimum. In: *Geophysical Research Letters* 35 (2008), Nr. 8. – Times Cited: 91 Kay, Jennifer E. L’Ecuyer, Tristan Gettelman, Andrew Stephens, Graeme O’Dell, Chris.
- [Kendall 1948] KENDALL, Maurice G.: Rank correlation methods. In: *Rank correlation methods*. (1948).
- [Kwok & Untersteiner 2011] KWOK, Ronald ; UNTERSTEINER, Norbert: The thinning of Arctic sea ice. In: *Physics today* 64 (2011), S. 36.
- [Lavergne & Eastwood 2012] LAVERGNE, T. ; EASTWOOD, S.: e-mail. 2012. – t.lavergne@met.no, s.eastwood@met.no.
- [Lavergne et al. 2010] LAVERGNE, T. ; KILLIE, M.A. ; EASTWOOD, S. ; BREIVIK, L.A.: Extending the CryoClim Arctic sea ice extent time series with operational

- OSI SAF products from 2008 onwards. In: *Norwegian Meteorological Institute note* (2010), Nr. 7.
- [Lutgens et al. 1995] LUTGENS, Frederick K. ; TARBUCK, Edward J. ; TASA, Dennis: *Essentials of geology*. Bd. 480. Prentice Hall, 1995.
- [Mann 1945] MANN, Henry B.: Nonparametric tests against trend. In: *Econometrica: Journal of the Econometric Society* (1945), S. 245–259.
- [Markus 2012] MARKUS, T.: *Arctic Sea Ice melt: Data Description*. <http://neptune.gsfc.nasa.gov/csb/index.php?section=54>. 12 2012. – last access: 14 January 2013.
- [Markus et al. 2009] MARKUS, T. ; STROEVE, J.C. ; MILLER, J.: Recent changes in Arctic sea ice melt onset, freezeup, and melt season length. In: *Journal of Geophysical Research* 114 (2009), Nr. C12, S. C12024.
- [Maslanik et al. 2011] MASLANIK, J. ; STROEVE, J. ; FOWLER, C. ; EMERY, W.: Distribution and trends in Arctic sea ice age through spring 2011. In: *Geophysical Research Letters* 38 (2011), Nr. 13, S. L13502.
- [Maslanik et al. 2007] MASLANIK, J.A. ; FOWLER, C. ; STROEVE, J. ; DROBOT, S. ; ZWALLY, J. ; YI, D. ; EMERY, W.: A younger, thinner Arctic ice cover: Increased potential for rapid, extensive sea-ice loss. In: *Geophysical Research Letters* 34 (2007), Nr. 24, S. L24501.
- [Maykut 1978] MAYKUT, Gary A.: Energy exchange over young sea ice in the central Arctic. In: *Journal of Geophysical Research* 83 (1978), Nr. C7, S. 3646–3658.
- [Maykut 1986] MAYKUT, Gary A.: *The surface heat and mass balance*. University of Washington, 1986.
- [Nicolaus et al. 2013] NICOLAUS, M. ; ARNDT, S. ; KATLEIN, C. ; MASLANIK, J. ; HENDRICKS, S.: Correction to: Changes in Arctic sea ice result in increasing light transmittance and absorption. In: *Geophysical Research Letters* (2013).
- [Nicolaus et al. 2010a] NICOLAUS, M. ; GERLAND, S. ; HUDSON, S.R. ; HANSON, S. ; HAAPALA, J. ; PEROVICH, D.K.: Seasonality of spectral albedo and transmittance as observed in the Arctic Transpolar Drift in 2007. In: *Journal of Geophysical Research* 115 (2010), Nr. C11, S. C11011.
- [Nicolaus et al. 2010b] NICOLAUS, M. ; HUDSON, S. R. ; GERLAND, S. ; MUNDERLOH, K.: A modern concept for autonomous and continuous measurements of

- spectral albedo and transmittance of sea ice. In: *Cold Regions Science and Technology* 62 (2010), Nr. 1, S. 14–28.
- [Nicolaus & Katlein 2013] NICOLAUS, M ; KATLEIN, C: Mapping radiation transfer through sea ice using a remotely operated vehicle (ROV). In: *The Cryosphere* 7 (2013), Nr. 3, S. 763–777.
- [Nicolaus et al. 2012] NICOLAUS, M. ; KATLEIN, C. ; MASLANIK, J. ; HENDRICKS, S.: Changes in Arctic sea ice result in increasing light transmittance and absorption. In: *Geophysical Research Letters* 39 (2012), Nr. 24, S. submitted.
- [NSIDC 2012] NSIDC: *National Snow & Ice Data Center (NSIDC)*. <http://nsidc.org/arcticseaicenews/files/2012/04/Figure5.png>; last visit: 10.06.2012, 11:52. 2012.
- [Perovich 2005] PEROVICH, D. K.: On the aggregate-scale partitioning of solar radiation in Arctic sea ice during the Surface Heat Budget of the Arctic Ocean (SHEBA) field experiment. In: *Journal of Geophysical Research-Oceans* 110 (2005), Nr. C3.
- [Perovich et al. 1998] PEROVICH, D. K. ; ROESLER, C. S. ; PEGAU, W. S.: Variability in Arctic sea ice optical properties. In: *Journal of Geophysical Research-Oceans* 103 (1998), Nr. C1, S. 1193–1208.
- [Perovich 1996] PEROVICH, D.K.: The Optical Properties of Sea Ice / DTIC Document. 1996. – Forschungsbericht.
- [Perovich et al. 2002] PEROVICH, DK ; GRENFELL, TC ; LIGHT, B. ; HOBBS, PV: Seasonal evolution of the albedo of multiyear Arctic sea ice. In: *Journal of Geophysical Research* 107 (2002), Nr. C10, S. 8044.
- [Perovich et al. 2011] PEROVICH, D.K. ; JONES, K.F. ; LIGHT, B. ; EICKEN, H. ; MARKUS, T. ; STROEVE, J. ; LINDSAY, R.: Solar partitioning in a changing Arctic sea-ice cover. In: *Annals of Glaciology* 52 (2011), Nr. 57, S. 192–196.
- [Perovich & Polashenski 2012] PEROVICH, D.K. ; POLASHENSKI, C.: Albedo evolution of seasonal Arctic sea ice. In: *Geophysical Research Letters* 39 (2012), Nr. 8, S. L08501.
- [Perovich & Richter-Menge 2009] PEROVICH, Donald K. ; RICHTER-MENGE, Jacqueline A.: Loss of Sea Ice in the Arctic*. In: *Annual Review of Marine Science* 1 (2009), S. 417–441.
- [Richter-Menge et al. 2011] RICHTER-MENGE, J. et al.: *Arctic Report Card 2010*. DIANE Publishing, 2011.

- [Rösel & Kaleschke 2012] RÖSEL, A. ; KALESCHKE, L.: Exceptional melt pond occurrence in the years 2007 and 2011 on the Arctic sea ice revealed from MODIS satellite data. In: *Journal of Geophysical Research-Oceans* 117 (2012).
- [Rösel et al. 2011] RÖSEL, A. ; KALESCHKE, L. ; BIRNBAUM, G.: Melt ponds on Arctic sea ice determined from MODIS satellite data using an artificial neural network. In: *The Cryosphere Discuss* 5 (2011), S. 2991–3024. – Integrated Climate Data Center (ICDC), CliSAP/KlimaCampus, University of Hamburg, Hamburg, Germany, <http://icdc.zmaw.de>.
- [Sedlar et al. 2011] SEDLAR, Joseph ; TJERNSTRÖM, Michael ; MAURITSEN, Thorsten ; SHUPE, Matthew D. ; BROOKS, Ian M. ; PERSSON, P Ola G. ; BIRCH, Cathryn E. ; LECK, Caroline ; SIREVAAG, Anders ; NICOLAUS, Marcel: A transitioning Arctic surface energy budget: the impacts of solar zenith angle, surface albedo and cloud radiative forcing. In: *Climate dynamics* 37 (2011), Nr. 7, S. 1643–1660.
- [Serreze & Barry 2005] SERREZE, Mark C. ; BARRY, Roger G.: *The Arctic climate system*. Bd. 22. Cambridge University Press, 2005.
- [Serreze et al. 2007] SERREZE, Mark C. ; HOLLAND, Marika M. ; STROEVE, Julienne: Perspectives on the Arctic’s shrinking sea-ice cover. In: *science* 315 (2007), Nr. 5818, S. 1533–1536.
- [Smedsrud et al. 2008] SMEDSRUD, L. H. ; SORTEBERG, A. ; KLOSTER, K.: Recent and future changes of the Arctic sea-ice cover. In: *Geophysical Research Letters* 35 (2008), Nr. 20. – Times Cited: 16 Smedsrud, Lars H. Sorteberg, Asgeir Kloster, Kjell.
- [Tschudi et al. 2008] TSCHUDI, M.A. ; MASLANIK, J.A. ; PEROVICH, D.K.: Derivation of melt pond coverage on Arctic sea ice using MODIS observations. In: *Remote Sensing of Environment* 112 (2008), Nr. 5, S. 2605–2614.
- [Weeks 2010] WEEKS, Willy: *On sea ice*. University of Alaska Press, 2010.
- [Wendler et al. 1997] WENDLER, Gerd ; ADOLPHS, Ute ; HAUSER, Adrian ; MOORE, Blake: On the surface energy budget of sea ice. In: *Journal of Glaciology-Only* 43 (1997), Nr. 143, S. 122–130.

Acknowledgements

First of all, I would like to thank my supervisor at AWI Dr. Marcel Nicolaus for introducing me to the topic as well as for the support, useful comments and remarks through the learning process of this master thesis.

Great thanks to Prof. Dr. Martin Claussen who was the first supervisor of this thesis and gave me the possibility for this external master thesis.

Thanks to James Maslanik for providing the ice type data sets, to Thorsten Markus for providing the melt and freeze onset data, to Thomas Lavernge for all his help with the OSI SAF data sets, and to Anja Rösel and Lars Kaleschke for their support with the melt pond fraction data.

Moreover, I would like to thank my office colleagues Kathrin Riemann-Campe, Michael Karcher and Frank Kauker for their patience with me, the fruitful discussions and the lot of fun during the working time.

Many thanks to the entire section of Sea ice physics at the Alfred-Wegener-Institut Helmholtz-Zentrum für Polar- und Meeresforschung in Bremerhaven for a nice working atmosphere, providing working appliance and resources as well as for a warm and friendly reception in Bremerhaven.

I would like to thank Ben Hörz for supporting me in every situation during the last years and who never lost faith in me and my ideas. Moreover, I would like to thank for proofreading.

Also many thanks to my brother Sebastian for being the best brother in every situation and proofreading this thesis.

Finally, special thanks to my parents who always support me whatever I do and wherever I go.

Erklärung zur Anfertigung und Veröffentlichung der vorliegenden Masterarbeit

Hiermit erkläre ich, dass ich die vorliegende Arbeit selbstständig verfasst und keine anderen als die angegebenen Hilfsmittel, insbesondere keine nicht genannten Internet-Quellen verwendet habe. Weiterhin versichere ich, dass ich diese Arbeit vorher nicht in einem anderen Prüfungsverfahren eingereicht habe. Die eingereichte schriftliche Fassung der Arbeit entspricht der auf dem Speichermedium.

Einer Veröffentlichung der Arbeit in der Bibliothek der Universität Hamburg stimme ich zu.

Hamburg, den 30.05.2013

Stefanie Arndt